Received: 3 March 2018 | Revised: 15 October 2018 | Accepted: 23 October 2018

DOI: 10.1111/ejn.14263

RESEARCH REPORT

WILEY EJN European Journal of Neuroscience FENS

Neuronal phase consistency tracks dynamic changes in acoustic spectral regularity

Adam M. Gifford[1] | **Michael R. Sperling**[2] | **Ashwini Sharan**[2] | **Richard J. Gorniak**[3] | **Ryan B. Williams**[4] | **Kathryn Davis**[5] | **Michael J. Kahana**[1,4] | **Yale E. Cohen**[1,6]

[1]Neuroscience Graduate Group, University of Pennsylvania, Philadelphia, Pennsylvania

[2]Jefferson Comprehensive Epilepsy Center, Department of Neurology, Thomas Jefferson University, Philadelphia, Pennsylvania

[3]Department of Radiology, Sidney Kimmel Medical College, Thomas Jefferson University, Philadelphia, Pennsylvania

[4]Department of Psychology, University of Pennsylvania, Philadelphia, Pennsylvania

[5]Department of Neurology, University of Pennsylvania, Philadelphia, Pennsylvania

[6]Departments of Otorhinolaryngology, Neuroscience, and Bioengineering, University of Pennsylvania, Philadelphia, Pennsylvania

Correspondence
Yale E. Cohen, Department of Otorhinolaryngology, Philadelphia, PA.
Email: ycohen@pennmedicine.upenn.edu

Funding information
DARPA Restoring Active Memory (RAM); Boucai Hearing Restoration Fund; NIDCD-NIH; NIMH-NIH

Abstract

The brain parses the auditory environment into distinct sounds by identifying those acoustic features in the environment that have common relationships (e.g., spectral regularities) with one another and then grouping together the neuronal representations of these features. Although there is a large literature that tests how the brain tracks spectral regularities that are predictable, it is not known how the auditory system tracks spectral regularities that are not predictable and that change dynamically over time. Furthermore, the contribution of brain regions downstream of the auditory cortex to the coding of spectral regularity is unknown. Here, we addressed these two issues by recording electrocorticographic activity, while human patients listened to tone-burst sequences with dynamically varying spectral regularities, and identified potential neuronal mechanisms of the analysis of spectral regularities throughout the brain. We found that the degree of oscillatory stimulus phase consistency (PC) in multiple neuronal-frequency bands tracked spectral regularity. In particular, PC in the delta-frequency band seemed to be the best indicator of spectral regularity. We also found that these regularity representations existed in multiple regions throughout cortex. This widespread reliable modulation in PC – both in neuronal-frequency space and in cortical space – suggests that phase-based modulations may be a general mechanism for tracking regularity in the auditory system specifically and other sensory systems more generally. Our findings also support a general role for the delta-frequency band in processing the regularity of auditory stimuli.

1 | INTRODUCTION

A fundamental goal of the auditory system is to parse the auditory environment into distinct perceptual representations (i.e., sounds); this process is often called "auditory scene analysis" (Bizley & Cohen, 2013; Bregman, 1990; McDermott, 2009; Shinn-Cunningham, 2008; Winkler, Denham, & Nelken, 2009). The auditory system accomplishes this feat, in part, by first identifying the acoustic features in the environment that have common relationships with one another and then grouping together the neuronal representations of these features. These common relationships can occur either at a particular time (e.g., a harmonic

Abbreviations: C_K, Kolmogorov complexity; ECoG, electrocorticographic; FDR, false-detection rate; HL, high gamma; *L*, length; PC, phase consistency; SL, subsequence length.

Edited by John Foxe. Reviewed by Julian Keil and Adam Snyder.

All peer review communications can be found with the online version of the article.

stack) or over time (e.g., a frequency sweep of increasing acoustic frequencies). When these common relationships relate to the frequency content of an acoustic stimulus, they are referred to as "spectral regularities".

A classic example of how spectral regularities can create distinct sounds is East African xylophone music (see Bregman, 1990). In this music, two musicians play a series of high- and low-frequency notes at a constant rhythm. Human listeners, though, do not hear the isochronous sound produced by each xylophone. Instead, they simultaneously hear one high-frequency sound that has an irregular rhythm and a second low-frequency sound that also has an irregular rhythm. In this example, spectral regularity is the acoustic feature that groups the stimuli into two distinct sounds and not the temporal pattern of each xylophone's notes.

The neuronal mechanisms that track spectral regularities and the cortical regions that are modulated by spectral regularity are not fully elucidated. Although there is an extensive literature on how the brain encodes the spectral regularity of a stimulus when the regularity is predictable (Barascud, Pearce, Griffiths, Friston, & Chait, 2016; Bendixen, Roeber, & Schroger, 2007; Dimitrijevic, John, & Picton, 2004; Fishman, Arezzo, & Steinschneider, 2004; Fuentemilla, Marco-Pallares, Munte, & Grau, 2008; Lakatos et al., 2013; Luo, Wang, Poeppel, & Simon, 2006; Micheyl, Tian, Carlyon, & Rauschecker, 2005; Southwell et al., 2017; Ulanovsky, Las, & Nelken, 2003; Winkler, Karmos, & Naatanen, 1996), it is unknown how the auditory system tracks an auditory stimulus when its spectral regularity is not predictable and changes dynamically over time. Further, the contributions of regions that are downstream of the core auditory cortex (Fishman et al., 2004; Lakatos et al., 2005, 2013; Micheyl et al., 2005; Ulanovsky et al., 2003) to spectral regularity have not been fully characterized. Thus, the goal of this study was to identify potential mechanisms by which the auditory and nonauditory cortices code dynamic changes in an auditory stimulus' spectral regularity.

We recorded electrocorticographic (ECoG) activity from electrodes distributed across the human cortex while patients listened passively to tone-burst sequences, whose spectral regularity changed dynamically over time. Throughout the cortex, we found that spectral regularity correlated with the phase consistency (PC) of the ECoG signal at a number of neuronal frequency bands; in particular, delta-band (<3 Hz) PC appeared to be the best indicator of spectral regularity. Because PC can dynamically track spectral regularity, it may facilitate the segregation of the auditory environment into distinct sounds, a finding consistent with the hypothesis that the delta band may have a general role in auditory scene analysis (Doelling, Arnal, Ghitza, & Poeppel, 2014; Giraud & Poeppel, 2012; Riecke, Sack, & Schroeder, 2015).

2 | MATERIALS AND METHODS

2.1 | Participants

Eleven participants (five females, four left-handed, mean age: 30.1 ± 12.8 years) with medically intractable epilepsy underwent surgery to implant subdural platinum recording electrodes on the cortical surface and into the brain parenchyma. In each case, clinical teams (at either the Hospital of the University of Pennsylvania or Thomas Jefferson University Hospital) determined electrode placement in order to localize epileptogenic brain regions. Institutional review boards at each hospital approved the research protocol. Informed consent was obtained from each participant prior to their participation in this study.

One participant was implanted twice (time between implantations: ~1 year) and participated in our experiment on both occasions. Because of the time between implantations, differences in electrode placement (i.e., the surgical team targeted different brain regions in each surgery) and because the patient was presented with unique tone-burst sequences (see below) during each experimental session, we treated the data obtained from the two implantations as independent data sets. Thus, we report data from twelve subjects.

2.2 | Experimental paradigm

This study tested how the brain tracks the spectral regularity of an acoustic stimulus. For our purposes, spectral regularities are probabilistically predictable patterns in the spectral content of an acoustic stimulus at a particular time (e.g., a harmonic stack) or over time (e.g., a frequency sweep). Here, we focused on spectral regularities over time.

To test how the brain tracked these spectral regularities, we constructed a sequence of tone bursts in which the acoustic frequency of the tone bursts changed pseudorandomly but the time between the tone bursts was constant. Hence, the spectral regularity of these tone-burst sequences changed dynamically, whereas the temporal regularity was constant. (The temporal regularity did not change because the tone-repetition rate was constant.) In the following sections, we describe (1) the construction of the auditory stimuli with dynamically changing spectral regularities; (2) how these stimuli were presented to the patients; (3) our data acquisition; and finally, (4) our approach to data analysis –both acoustic and electrophysiological– to identify neuronal correlates of spectral regularity in the ECoG signal.

2.3 | Construction of auditory stimulus

We constructed tone-burst sequences with a pseudorandom distribution of acoustic-frequency values. The distribution of these frequency values was determined through an

m-sequence, a pseudorandom binary sequence that is generated using a linear feedback algorithm (Buracas & Boynton, 2002; Golomb, 1982; Kvale & Schreiner, 1995). The length (L) of each m-sequence was $L = 2^n - 1$, where n is the order of the sequence and the bit level of the shift register that defined the memory length of the linear feedback (Buracas & Boynton, 2002; Golomb, 1982). We first generated 4 m-sequences of orders 5, 6, 7, and 8 and concatenated together these 4 m-sequences. This concatenated m-sequence contained 476 binary values. The acoustic-frequency distribution of the tone bursts in a sequence was constructed by mapping each of these 476 binary values to one of two different frequency values: 1,000 Hz (F_1) or 1,029 Hz (F_2; ½ semitone above F_1); within a tone-burst sequence, F_1 and F_2 occurred with approximately equal probability. This process generated 48 independent m- (tone-burst) sequences.

The duration of each tone-burst sequence was 47.6 s; each of the 476 tone bursts had a 50-ms duration (5-ms $\cos^2$ ramp) with a 50-ms inter-tone interval (10 Hz onset-to-onset interval). Each tone-burst sequence was preceded by 22.4 s of silence (70-s total duration). We presented the tone-burst sequences at 65 dB SPL and delivered the sequences through calibrated insert-ear buds (ER-MC5, Etymotic) that were connected to a laptop (either a 15-inch MacBook Pro or a 13-inch MacBook Air, Apple). We chose the tone-burst frequencies and presentation rate to maximize the number of tone bursts in the stimulus, while minimizing the possibility that subjects would segregate the stimulus into two separate sounds (Bregman, 1990; Cusack, 2005).

2.4 | Stimulus presentation

Subjects listened to these tone-burst sequences while they rested comfortably in their hospital beds. They could read but were asked to refrain from speaking. During each testing session, participants listened to 10 different tone-burst sequences that were chosen randomly from our test bank of 48 sequences. Sessions were separated by at least 1 min and at most by 12 days. Subjects completed 2–6 sessions.

2.5 | Data acquisition and preprocessing

Subdural electrodes were arranged in either grids or strips; each electrode contact was separated by 10 mm. Depth electrodes contained 6–8 contacts and were separated by 8 mm; the depth electrodes were located primarily in the medial temporal lobes. We localized electrodes to specific brain regions by co-registering postoperative computed-tomography scans with postoperative MRI scans using the FSL (FMRIB [Functional MRI of the Brain] Software Library], BET (Brain Extraction Tool), and FLIRT (FMRIB Linear Image Registration Tool) software packages. These electrode locations were then mapped to Talairach space using indirect stereotactic techniques and the OsiriX Imaging Software DICOM viewer package (Burke et al., 2013).

We assigned anatomical labels to these electrode locations based on the Desikan-Killliany (D-K) atlas (Desikan et al., 2006; Ramayya, Pedisich, & Kahana, 2015). Following from Ramayya et al. (2015), we further defined regions of interest based on these anatomical labels. The "orbitofrontal cortex" included D-K regions medial orbitofrontal and lateral orbitofrontal cortex. The "dorsolateral prefrontal cortex" included D-K regions rostral middle frontal and caudal middle frontal cortex. The "ventrolateral prefrontal cortex" included D-K regions pars triangularis, pars opercularis, and pars orbitalis. The "anterior medial frontal cortex" included D-K regions superior frontal cortex, rostral anterior cingulate, and caudal anterior cingulate. The "posterior medial frontal cortex" included D-K regions paracentral cortex, posterior cingulate, and isthmus cingulate. "Sensorimotor cortex" included D-K regions precentral and postcentral cortex. "Parietal cortex" included D-K regions superior parietal, supramarginal, and inferior parietal cortex. "Temporal cortex" included D-K regions bank of the superior temporal sulcus, transverse temporal cortex, middle temporal cortex, inferior and superior temporal cortex. "Other temporal cortex" included all of the temporal cortex except for the superior temporal cortex; the superior temporal cortex was the closest D-K region to the primary auditory cortex. "Fusiform cortex" included D-K region fusiform cortex. "Occipital cortex" included D-K regions cuneate, lateroccipital, lingual and pericalcarine cortex. Finally, the "medial temporal lobe" included D-K regions entorhinal and parahippocampal cortex and depth electrodes labeled as hippocampus or entorhinal, perirhinal and parahippocampal cortex by the clinical radiologist.

We recorded ECoG signals with either a Nicolet or a Nihon Kohden electroencephalogram system (Burke et al., 2013). ECoG signals were sampled at 1,000 Hz. A testing laptop sent ±5-V analog pulses, via an optical isolator, to open lines in the clinical-recording system to align stimulus- and task-related events with the ECoG recordings.

We minimized reference-line and volume–conduction confounds with a bipolar-referencing scheme (Burke et al., 2013; Nunez & Srinivasan, 2006) in which we subtracted the signals from each pair of immediately adjacent electrode contacts on the same grid, strip, or depth electrode (Anderson, Rajagovindan, Ghacibeh, Meador, & Ding, 2010; Burke et al., 2013). The location of these bipolar signals was defined as halfway between each electrode-contact pair.

When we tested high-gamma (HG) activity, we down-sampled ECoG activity to 500 Hz and band-pass filtered it between 70 and 200 Hz (2nd-order zero-phase-shift Butterworth filters). When we tested ECoG sensitivity to spectral regularities (see Section 2.6), we down-sampled

(a)

Pattern	F_1 F_1 F_1 F_1 F_1 F_1 F_1 F_2	F_1 F_2	F_1 F_2 F_1	F_1 F_2 F_2 F_1
Simplest form	$7\bullet\{F_1\}$	$7\bullet\{F_1\}\{F_2\}$	$3.5\bullet\{F_1F_2\}$	$\{F_1F_2F_1F_1F_2F_2F_1\}$
Regularity	High	High	Medium	Low
Regularity ($1/C_K$)	1.66	1.25	0.997	0.55

(b)

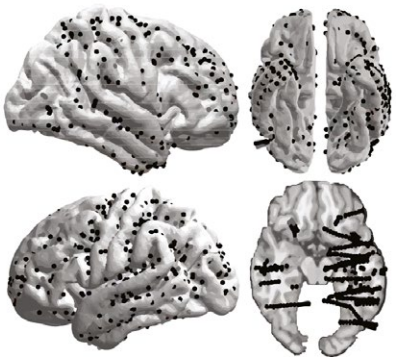

FIGURE 1 Calculation of regularity metric and brain summary plot. (a) Summary table illustrating different local configurations of F_1 and F_2 within an auditory stimulus and their respective regularity ($1/C_K$) values. First row: an example pattern of the distribution of tone bursts F_1 and F_2 in an auditory stimulus. Four different subsequences with different configurations of F_1 and F_2 are highlighted in red, orange, green, and blue from left to right. Each subsequence consisted of 7 tone bursts. Second row: simplification of highlighted subsequences into shorter, repeated patterns. The red-highlighted subsequence is the "most regular" because it can by simplified into seven repeats of the shorter pattern ($7\bullet\{F_1\}$). The orange-highlighted subsequence is the next most regular because of the frequency change in the last tone ($6\bullet\{F_1\}\{F_2\}$).The green-highlighted subsequence is less regular still because it can only be simplified into 3.5 repeats of the shorter pattern ($3.5\bullet\{F_1–F_2\}$). The blue-highlighted subsequence is the least regular because it cannot be simplified into a pattern shorter than its entire length. Fourth row: quantitative measure of regularity using the $1/C_K$ metric. (b) Brain plots depict the locations of electrodes (black dots) across all subjects on an average-subject brain. The brains are oriented such that the left side of the brain is shown on the left and the right side is on the right. The brain plot in the lower shows the underside of the brain with the lower brainstem removed

ECoG activity to 500 Hz and either notch-filtered (4th-order zero-phase-shift Butterworth filter; stop-band: 58–62 Hz) it to remove power-line noise for wideband analyses or band-pass filtered (4th-order zero-phase-shift Butterworth filters with ~3–4-Hz pass bands) it for frequency-band-specific analyses. To help to ensure that our findings were not due to the particulars (e.g., systematic phase shifts) of our filtering technique (Widmann, Schroger, & Maess, 2015), we redid portions of our analysis using low-order zero-phase shift Butterworth filters (1st-order Butterworth filters in the forward and reverse direction, total order = 2) and found comparable results (data not shown).

2.6 | Approach to data analysis

We tested how ECoG activity in response to the last ("test") tone burst in a subsequence was modulated (i.e., *conditioned*) by the spectral regularity of the *previous* tone bursts; a subsequence is a subset of tone bursts within a larger tone-burst sequence. We tested this modulation over different timescales (Denham & Winkler, 2006; Fuentemilla, Marco-Pallarés, & Grau, 2006; Fuentemilla et al., 2008; Hsiao, Wu, Ho, & Lin, 2009; Lakatos et al., 2013; Patel & Balaban, 2000; Winkler et al., 2009). This approach was advantageous because we did not have to make any assumptions about how the brain might encode spectral regularity.

To get insight into this approach, consider the last F_2 (the test tone burst; in bold font) in these two tone-burst sequences:

1. F_2—F_1—F_2—F_1—$\mathbf{F_2}$
2. F_2—F_1—F_1—F_2—$\mathbf{F_2}$

The first sequence has more spectral regularity (i.e. it is more predictable) than the second sequence because F_1 and F_2 alternate in the first sequence but do not alternate in the second sequence. Because of this difference in regularity, we hypothesized that ECoG activity elicited by the test-tone-burst F_2 in the more regular sequence should be different than activity elicited by the same F_2 in the less regular subsequence.

2.7 | Analysis of the acoustic-frequency regularity of the tone-burst sequences

The time scale of spectral regularity was based on the length of a tone-burst subsequence. The "length" of a subsequence is the number of tone bursts in the subsequence. For a given length l, each tone burst in the subsequence was included as the final tone burst of its own subsequence, except for the first $l-1$ tone bursts.

By construction, each tone-burst sequence contained ≥1 occurrences of all possible subsequences up to a subsequence $l = 7$ (i.e., between 200–700 ms or 2–7 tone bursts). As a consequence, the local spectral regularity of the sequence changed dynamically over time and over different timescales. Because each of the 48 m-sequences (see above) had an odd number of tone bursts, there was a slight imbalance in the number of tone bursts with frequencies F_1 and F_2.

1. *Kolmogorov complexity to quantify spectral regularity.* Our primary metric for regularity was based on the Kolmogorov complexity (Kaspar & Schuster, 1987; Kolmogorov, 1963; Lempel & Ziv, 1976), C_K. Here, we define "regularity" as $1/C_K$ (Figure 1a). C_K is a measure of randomness that quantifies the extent to which a subsequence's configuration of F_1 and F_2 tone bursts can be reduced to repeats of simpler (shorter)

configurations. This regularity algorithm performs two operations: copy or insert. For a given tone-burst subsequence, the algorithm determined whether future configurations of tone bursts within the subsequence can be (1) *copied* from the past "vocabulary" of tone-burst configurations or (2) if a configuration needed to be *inserted* as a new configuration. The number of times a new configuration was inserted into the vocabulary of the subsequence determines the regularity of the subsequence. The C_K value is a normalized metric of the number of insertions: $C_K = \frac{1}{n} i \log_2 n$, where i is the number of insertions, and n is the length of the subsequence.

As an example of how this metric works, consider the following four subsequences:

1. F_1—F_1—F_1—F_1—F_1—F_1—F_1
2. F_1—F_1—F_1—F_1—F_1—F_1—F_2
3. F_1—F_2—F_1—F_2—F_1—F_2—F_1
4. F_1—F_2—F_1—F_1—F_2—F_2—F_1

The first subsequence requires an initial insertion of the first F_1, but all of the subsequent patterns of future tone bursts in the subsequence can simply be copied from the existing vocabulary of tone bursts. Because the subsequence ends on a copy operation, an additional insertion operation is included to end the subsequence, for a total of two insertion operations. The second subsequence also requires two insertion operations: one for the first F_1 tone at the beginning of the subsequence and one for the first F_2 tone at the end. Consequently, both of these subsequences should have identical C_K values. However, to better reflect our intuition that the first subsequence is less complex (i.e., more regular) than the second, we modified the algorithm such that we added 0.5 to the total number of insertions if a subsequence ended with a copy operation. Thus, the first subsequence has the higher $1/C_K$ (regularity) value (1.66) and the second subsequence has a slightly lower regularity value (1.25).

Next, let us consider subsequences (3) and (4). The third subsequence requires 2.5 insertions, corresponding to a slightly more complex pattern of repeating pairs of F_1—F_2. Consequently, it has a lower regularity value than the first two subsequences (0.997). Finally, the fourth subsequence requires 4.5 insertions and, thus, has the lowest regularity value (0.554).

There are several other important properties to note about the nature of this C_K regularity metric. First, the value of C_K depends on the reading direction of the subsequence. For instance, the second and fourth subsequences in the previous example would have different regularity metrics if the subsequence is reversed (1.25 and 0.554 in the forward direction compared to 0.997 and 0.623 in the reverse, respectively). Second, C_K values for subsequences of different lengths cannot be directly compared for lengths <1,000 tone bursts (Kaspar & Schuster, 1987). However, C_K can be compared directly for subsequences that have the same length. Nonetheless, if subsequences have the same "type" of combinations of F_1 and F_2 but have different lengths, they have similar C_K values, relative to other subsequences of the same length. Our use of this metric in subsequent analyses focused solely on scenarios in which we tested responses to subsequences of the same length.

For practical purposes, we focused our ECoG analyses on subsequences that had a length of ≤7 tone bursts. We chose this constraint to minimize redundancy in tests across different subsequence lengths (SLs) and to maximize the number of unique $1/C_K$ values that we could evaluate; the number of unique values scales linearly with SL. Furthermore, because of our stimulus design, we did not have the statistical power to sample all possible subsequences for lengths >7. Figure 2 is a complete list of all unique local configurations of subsequences with length of 7, along with the mean probabilities of their occurrences across auditory stimuli and their associated $1/C_K$ values.

2. *Other measures of spectral regularity.* To help to ensure that our findings were robust and not wholly dependent on the regularity Kolmogorov metric, we also quantified subsequence regularity with three other metrics: tone-burst proportion, Shannon entropy, and a "sub-symmetry" metric

The tone-burst-proportion metric was the proportion of F_1 tone bursts in each subsequence.

Shannon entropy measures the expected value of information content in a sequence of events (Shannon, 1948; Shannon & Weaver, 1949). Shannon entropy was defined as: $E = \sum_{j=1}^{k} P(F_j) \log_2 P(F_j)$, $k = 2$ is the number of different tone-burst frequencies, F_j is the identity of the acoustic frequency of a tone burst, and $P(F_j)$ is the probability of tone-burst F_j in the subsequence.

The final metric quantified the number of sub-symmetries in each subsequence (Alexander & Carey, 1968). To calculate the number of sub-symmetries, we first counted the number of times a length-m pattern of F_1 and F_2 tone bursts within a subsequence was symmetrical about a "center" tone burst. For example, in the subsequence F_1—F_2—F_1—F_2, the shorter subsequences F_1—F_2—F_1 and F_2—F_1—F_2 are symmetric about their center tone burst (F_2 and F_1, respectively). Formally, we defined the total number of sub-symmetries as $S = \sum_{m=1}^{n} \sum_{j=1}^{n-j+1} s_j$, where n is the SL, j cycles the number of F_1 and F_2 patterns of length m in the subsequence (total of $n - j + 1$), and s_j is a binary value that depends on the identity of each F_1 and F_2 pattern (i.e., F_j—F_{j+1}—…F_m). If a subsequence of tone bursts was symmetrical about its center, $s_j = 1$, otherwise $s_j = 0$.

Local Configuration	P	$1/C_K$	Local Configuration	P	$1/C_K$
F_1–F_1–F_1–F_1–F_1–F_1–F_1	0.0024	1.66	F_2–F_1–F_1–F_1–F_1–F_1–F_1	0.0065	0.997
F_1–F_1–F_1–F_1–F_1–F_1–F_2	0.0065	1.25	F_2–F_1–F_1–F_1–F_1–F_1–F_2	0.0084	0.831
F_1–F_1–F_1–F_1–F_1–F_2–F_1	0.0086	0.997	F_2–F_1–F_1–F_1–F_1–F_2–F_1	0.0084	0.712
F_1–F_1–F_1–F_1–F_1–F_2–F_2	0.0063	0.997	F_2–F_1–F_1–F_1–F_1–F_2–F_2	0.0086	0.712
F_1–F_1–F_1–F_1–F_2–F_1–F_1	0.010	0.997	F_2–F_1–F_1–F_1–F_2–F_1–F_1	0.0063	0.712
F_1–F_1–F_1–F_1–F_2–F_1–F_2	0.0065	0.997	F_2–F_1–F_1–F_1–F_2–F_1–F_2	0.0083	0.712
F_1–F_1–F_1–F_1–F_2–F_2–F_1	0.0083	0.831	F_2–F_1–F_1–F_1–F_2–F_2–F_1	0.0083	0.712
F_1–F_1–F_1–F_1–F_2–F_2–F_2	0.0065	0.997	F_2–F_1–F_1–F_1–F_2–F_2–F_2	0.0088	0.712
F_1–F_1–F_1–F_2–F_1–F_1–F_1	0.0086	0.997	F_2–F_1–F_1–F_2–F_1–F_1–F_1	0.0066	0.623
F_1–F_1–F_1–F_2–F_1–F_1–F_2	0.0079	0.997	F_2–F_1–F_1–F_2–F_1–F_1–F_2	0.0085	0.712
F_1–F_1–F_1–F_2–F_1–F_2–F_1	0.0083	0.997	F_2–F_1–F_1–F_2–F_1–F_2–F_1	0.0064	0.712
F_1–F_1–F_1–F_2–F_1–F_2–F_2	0.0065	0.831	F_2–F_1–F_1–F_2–F_1–F_2–F_2	0.0011	0.623
F_1–F_1–F_1–F_2–F_2–F_1–F_1	0.0082	0.712	F_2–F_1–F_1–F_2–F_2–F_1–F_1	0.0064	0.712
F_1–F_1–F_1–F_2–F_2–F_1–F_2	0.0084	0.712	F_2–F_1–F_1–F_2–F_2–F_1–F_2	0.0085	0.623
F_1–F_1–F_1–F_2–F_2–F_2–F_1	0.0084	0.831	F_2–F_1–F_1–F_2–F_2–F_2–F_1	0.0063	0.623
F_1–F_1–F_1–F_2–F_2–F_2–F_2	0.0069	0.997	F_2–F_1–F_1–F_2–F_2–F_2–F_2	0.0095	0.712
F_1–F_1–F_2–F_1–F_1–F_1–F_1	0.0086	0.712	F_2–F_1–F_2–F_1–F_1–F_1–F_1	0.0083	0.712
F_1–F_1–F_2–F_1–F_1–F_1–F_2	0.0066	0.712	F_2–F_1–F_2–F_1–F_1–F_1–F_2	0.0084	0.712
F_1–F_1–F_2–F_1–F_1–F_2–F_1	0.010	0.997	F_2–F_1–F_2–F_1–F_1–F_2–F_1	0.0066	0.712
F_1–F_1–F_2–F_1–F_1–F_2–F_2	0.0061	0.831	F_2–F_1–F_2–F_1–F_1–F_2–F_2	0.0085	0.623
F_1–F_1–F_2–F_1–F_2–F_1–F_1	0.0083	0.831	F_2–F_1–F_2–F_1–F_2–F_1–F_1	0.0090	0.831
F_1–F_1–F_2–F_1–F_2–F_1–F_2	0.0065	0.997	F_2–F_1–F_2–F_1–F_2–F_1–F_2	0.0073	0.997
F_1–F_1–F_2–F_1–F_2–F_2–F_1	0.010	0.712	F_2–F_1–F_2–F_1–F_2–F_2–F_1	0.0066	0.712
F_1–F_1–F_2–F_1–F_2–F_2–F_2	0.0067	0.712	F_2–F_1–F_2–F_1–F_2–F_2–F_2	0.0072	0.712
F_1–F_1–F_2–F_2–F_1–F_1–F_1	0.0082	0.712	F_2–F_1–F_2–F_2–F_1–F_1–F_1	0.0066	0.554
F_1–F_1–F_2–F_2–F_1–F_1–F_2	0.0065	0.712	F_2–F_1–F_2–F_2–F_1–F_1–F_2	0.0098	0.554
F_1–F_1–F_2–F_2–F_1–F_2–F_1	0.0085	0.712	F_2–F_1–F_2–F_2–F_1–F_2–F_1	0.0064	0.623
F_1–F_1–F_2–F_2–F_1–F_2–F_2	0.0084	0.712	F_2–F_1–F_2–F_2–F_1–F_2–F_2	0.0084	0.712
F_1–F_1–F_2–F_2–F_2–F_1–F_1	0.0084	0.712	F_2–F_1–F_2–F_2–F_2–F_1–F_1	0.0064	0.623
F_1–F_1–F_2–F_2–F_2–F_1–F_2	0.0064	0.712	F_2–F_1–F_2–F_2–F_2–F_1–F_2	0.011	0.712
F_1–F_1–F_2–F_2–F_2–F_2–F_1	0.0084	0.831	F_2–F_1–F_2–F_2–F_2–F_2–F_1	0.0065	0.623
F_1–F_1–F_2–F_2–F_2–F_2–F_2	0.0080	0.997	F_2–F_1–F_2–F_2–F_2–F_2–F_2	0.0076	0.712
F_1–F_2–F_1–F_1–F_1–F_1–F_1	0.0064	0.712	F_2–F_2–F_1–F_1–F_1–F_1–F_1	0.0085	0.997
F_1–F_2–F_1–F_1–F_1–F_1–F_2	0.011	0.623	F_2–F_2–F_1–F_1–F_1–F_1–F_2	0.0064	0.831
F_1–F_2–F_1–F_1–F_1–F_2–F_1	0.0064	0.712	F_2–F_2–F_1–F_1–F_1–F_2–F_1	0.0082	0.712
F_1–F_2–F_1–F_1–F_1–F_2–F_2	0.0086	0.623	F_2–F_2–F_1–F_1–F_1–F_2–F_2	0.0084	0.712
F_1–F_2–F_1–F_1–F_2–F_1–F_1	0.0066	0.712	F_2–F_2–F_1–F_1–F_2–F_1–F_1	0.0085	0.712
F_1–F_2–F_1–F_1–F_2–F_1–F_2	0.010	0.623	F_2–F_2–F_1–F_1–F_2–F_1–F_2	0.0066	0.712
F_1–F_2–F_1–F_1–F_2–F_2–F_1	0.0064	0.554	F_2–F_2–F_1–F_1–F_2–F_2–F_1	0.0085	0.712
F_1–F_2–F_1–F_1–F_2–F_2–F_2	0.0081	0.554	F_2–F_2–F_1–F_1–F_2–F_2–F_2	0.0077	0.712
F_1–F_2–F_1–F_2–F_1–F_1–F_1	0.0086	0.712	F_2–F_2–F_1–F_2–F_1–F_1–F_1	0.0082	0.712
F_1–F_2–F_1–F_2–F_1–F_1–F_2	0.0088	0.712	F_2–F_2–F_1–F_2–F_1–F_1–F_2	0.0064	0.712
F_1–F_2–F_1–F_2–F_1–F_2–F_1	0.0065	0.997	F_2–F_2–F_1–F_2–F_1–F_2–F_1	0.011	0.997
F_1–F_2–F_1–F_2–F_1–F_2–F_2	0.0073	0.831	F_2–F_2–F_1–F_2–F_1–F_2–F_2	0.0064	0.831
F_1–F_2–F_1–F_2–F_2–F_1–F_1	0.0082	0.623	F_2–F_2–F_1–F_2–F_2–F_1–F_1	0.0085	0.831
F_1–F_2–F_1–F_2–F_2–F_1–F_2	0.0086	0.712	F_2–F_2–F_1–F_2–F_2–F_1–F_2	0.0062	0.997
F_1–F_2–F_1–F_2–F_2–F_2–F_1	0.0065	0.712	F_2–F_2–F_1–F_2–F_2–F_2–F_1	0.010	0.712
F_1–F_2–F_1–F_2–F_2–F_2–F_2	0.0074	0.712	F_2–F_2–F_1–F_2–F_2–F_2–F_2	0.0067	0.712
F_1–F_2–F_2–F_1–F_1–F_1–F_1	0.0065	0.712	F_2–F_2–F_2–F_1–F_1–F_1–F_1	0.0084	0.997
F_1–F_2–F_2–F_1–F_1–F_1–F_2	0.0083	0.623	F_2–F_2–F_2–F_1–F_1–F_1–F_2	0.0082	0.831
F_1–F_2–F_2–F_1–F_1–F_2–F_1	0.0066	0.623	F_2–F_2–F_2–F_1–F_1–F_2–F_1	0.0085	0.712
F_1–F_2–F_2–F_1–F_1–F_2–F_2	0.0097	0.712	F_2–F_2–F_2–F_1–F_1–F_2–F_2	0.0064	0.712
F_1–F_2–F_2–F_1–F_2–F_1–F_1	0.0064	0.623	F_2–F_2–F_2–F_1–F_2–F_1–F_1	0.0082	0.831
F_1–F_2–F_2–F_1–F_2–F_1–F_2	0.0085	0.712	F_2–F_2–F_2–F_1–F_2–F_1–F_2	0.0085	0.997
F_1–F_2–F_2–F_1–F_2–F_2–F_1	0.0062	0.712	F_2–F_2–F_2–F_1–F_2–F_2–F_1	0.0084	0.997
F_1–F_2–F_2–F_1–F_2–F_2–F_2	0.011	0.623	F_2–F_2–F_2–F_1–F_2–F_2–F_2	0.0066	0.997
F_1–F_2–F_2–F_2–F_1–F_1–F_1	0.0063	0.712	F_2–F_2–F_2–F_2–F_1–F_1–F_1	0.010	0.997
F_1–F_2–F_2–F_2–F_1–F_1–F_2	0.0085	0.712	F_2–F_2–F_2–F_2–F_1–F_1–F_2	0.0065	0.831
F_1–F_2–F_2–F_2–F_1–F_2–F_1	0.0086	0.712	F_2–F_2–F_2–F_2–F_1–F_2–F_1	0.0082	0.997
F_1–F_2–F_2–F_2–F_1–F_2–F_2	0.0085	0.712	F_2–F_2–F_2–F_2–F_1–F_2–F_2	0.0065	0.997
F_1–F_2–F_2–F_2–F_2–F_1–F_1	0.0064	0.712	F_2–F_2–F_2–F_2–F_2–F_1–F_1	0.010	0.997
F_1–F_2–F_2–F_2–F_2–F_1–F_2	0.0085	0.712	F_2–F_2–F_2–F_2–F_2–F_1–F_2	0.0062	0.997
F_1–F_2–F_2–F_2–F_2–F_2–F_1	0.0079	0.831	F_2–F_2–F_2–F_2–F_2–F_2–F_1	0.0085	1.25
F_1–F_2–F_2–F_2–F_2–F_2–F_2	0.0077	0.997	F_2–F_2–F_2–F_2–F_2–F_2–F_2	0.0081	1.66

FIGURE 2 Complete list of local configurations of F_1 and F_2. For subsequence length = 7, each unique configuration (first column), the mean probabilities of occurrence across auditory stimuli (second column), and associated $1/C_K$ values (third column) is listed. The standard deviation for the probabilities across stimuli is ≤0.003 for all configurations

Even though each of these metrics are independent measures of spectral regularity, because they quantify the same underlying structure, each is highly correlated with $1/C_K$ (tone-burst proportion: Spearman $\rho = 0.41$, $p = 1.9E{-}6$; df = 126; Shannon entropy: Spearman $\rho = -0.41$, $p = 1.9E{-}6$; df = 126; and sub-symmetry metric: Spearman $\rho = 0.66$, $p = 2.6E{-}17$; df = 126).

2.8 | Analysis of neuronal correlates of spectral regularity in the ECoG signal

We restricted our analysis of spectral regularity to subsequences of 2–7 tone bursts (i.e., timescales between 200–700 ms); there were at least 20 total repetitions of each subsequence. Our analysis window started 500 ms after stimulus onset (i.e., after presentation of the first 5 50-ms tone bursts [each of which is separated by a 50-ms inter-tone interval]) to minimize the effects of stimulus onset on our measures of spectral regularity. In these analyses of the ECoG signals, we did not correct for multiple comparisons across electrodes for each subject. Instead, we used randomization procedures to estimate the false-positive rates. Also, we assessed the reliability of our results by testing the proportions of significant electrodes across subjects against the false-positive rate.

Analogous to that described in our quantification of the spectral regularity of a tone-burst sequence (see Section 2.7), we conducted a sliding-window analysis of an ECoG signal, after we discarded the response to the first 500-ms (i.e., the first 5 tone bursts). This analysis started at tone-burst l, where l is the length of the tested subsequences (as noted above). For example, if $l = 7$, the first test tone burst was the seventh tone (excluding first 5 discarded tone bursts). Every tone burst from tone l to the last tone burst in a sequence was a test tone burst in one of the analyses. ECoG data was analyzed as a function of the length l subsequence that included the current test tone burst and the immediately previous $l-1$ tones.

Our strategy was to first conduct a whole-brain analysis, which used all the electrodes from all of our patients (Figure 1b), and then to identify the neuronal oscillatory frequencies that were modulated by spectral regularity. After identifying those frequencies, we did band-specific analyses that allowed the identification of significant individual electrodes and, ultimately, an identification of brain areas that had a reliable number of significant electrodes.

Admittedly, this is a very conservative approach. However, we chose this strategy to be as unbiased as possible: using a whole-brain analysis, we could identify frequency bands of interest and then probe the reliability of individual electrodes and brain regions. This approach also minimized the issue of correcting for multiple comparisons (and the subsequent loss of statistical power) if we had to evaluate how individual electrodes were modulated across a large set of frequency bands.

2.8.1 | Identifying neuronal oscillatory frequencies that were modulated by spectral regularity

To identify those neuronal frequency bands that were modulated by spectral regularity, we first compared the ECoG signal that was elicited by "regular" subsequences in which all of the tone frequencies were the same (e.g., F_1—F_1—F_1 or F_2—F_2—F_2—F_2) with those elicited by one of two different classes of "irregular" subsequences. The first class were those subsequences in which all of the tone frequencies were the same except for the last ("deviant") one (e.g., F_2—F_2—F_2—F_1 or F_1—F_1—F_1—F_2). The second class were those subsequences in which acoustic frequency of the tone bursts alternated (e.g., F_1—F_2—F_1—F_2).

After aligning the ECoG signals relative to the onset of a tone-burst sequence, we performed a wavelet decomposition (wave number 6; including 22-s buffers of pre- and post-sequence ECoG activity relative to the onset of the tone-burst sequence; 35 frequencies between 0.5–200 Hz, evenly spaced on a $\log_2$ scale) to yield instantaneous power and phase responses as a function of time.

To test whether ECoG power was modulated by spectral regularity, we computed the grand-mean power of the ECoG signal that was elicited by the target tone burst across all of the electrodes for each subject and tested whether power was differentially modulated by subsequence regularity (signed-rank tests; H_0: ECoG power values were the same for the regular subsequences and for the irregular subsequences). This analysis was conducted as a function of SL and neuronal frequency.

Next, we tested whether the inter-trial PC (a bias-free measure of PC) (Vinck, van Wingerden, Womelsdorf, Fries, & Pennartz, 2010) of the ECoG signal was modulated by spectral regularity. PC is defined as: $\frac{2}{N(N-1)} \sum_{j=1}^{N-1} \sum_{k=(j+1)}^{N} f(\theta_j,\theta_k)$, with $f(\varphi,\omega) = \cos(\varphi)\cos(\omega) + \sin(\varphi)\sin(\omega)$. N is the number of tone-burst sequences and θ_j and θ_k are the relative phases from the ECoG signal elicited by two different target tone bursts on the *same electrode*.

For each electrode, we collected all of the ECoG signals that were generated in response to a particular SL and a particular subsequence regularity. Next, across all possible pairs of ECoG signals, we calculated a PC value (see below). For example, if we collected N trials from a single electrode, we calculated $\binom{N}{2}$ combinations. We report the average value of those pairwise calculations, either grand averaged over all electrodes or for individual electrodes.

A PC value was calculated for each pair of ECoG signals in the follow manner. Relative to the onset of a test tone burst, we first calculated an instantaneous measure of phase over a 100-ms time window (i.e., the 50-ms duration of the test tone and the immediately preceding 50-ms silent gap) for each ECoG signal. Across a pair of ECoG signals, we then calculated the instantaneous PC values and averaged together those values.

We independently compared ECoG signals elicited by the regular subsequences with the ECoG signals elicited by the two classes of irregular subsequences. Raw *p*-values were false-discovery-rate (FDR) corrected across SL and neuronal frequency (Q = 0.05) (Benjamini & Hochberg, 1995). We identified those frequency bands that were consistently modulated by spectral regularity across the majority (≥4) of SLs.

2.8.2 | Band-specific analyses measuring modulations to spectral regularity

Next, we correlated the instantaneous PC and amplitude responses of band-limited ECoG signals with our metrics of subsequence regularity (e.g., $1/C_K$; see Analysis of the acoustic-frequency regularity of the tone-burst sequences above). This analysis was restricted to those frequency bands that were identified as being modulated by spectral regularity (see *Identifying neuronal oscillatory frequencies that were modulated by spectral regularity*) as well as data from the HG band (70–200 Hz), due to its purported relationship with neuronal-spiking activity (Mukamel et al., 2005; Ray, Crone, Niebur, Franaszczuk, & Hsiao, 2008; Ray & Maunsell, 2011).

We computed these phase and amplitude responses by first band-pass filtering the ECoG signals and computing the Hilbert transform (2-s ECoG buffers). To facilitate across-subject comparisons, we computed the subsequence-aligned average PC responses across electrodes for each subject. Next, after applying a Fisher *z*-transform, we *z*-scored the averaged responses, using the mean and standard deviation of the population of PC responses to all local configurations of F_1 and F_2. Finally, across subjects, a Spearman correlation (ρ) evaluated the null hypothesis that there was not a monotonic association between the *z*-scored PC responses and a metric of spectral regularity. An analogous analysis evaluated the association between spectral regularity and *z*-scored log amplitude; however, we did not apply the Fisher transform prior to *z*-scoring.

We identified individual electrodes and, subsequently, brain regions (see next section), that were reliably modulated by spectral regularity, by calculating the Spearman correlations for PC and amplitude as a function of spectral regularity on an electrode-by-electrode basis. We estimated the false-positive rate by computing a null distribution of 1,000 Spearman correlations; this distribution was calculated by randomizing the relationship between response (PC or amplitude) and local configuration. An electrode was "significant" if its actual correlation was greater than random chance (two-tail comparison, false-positive rate = 0.05). Because this analysis was conducted on an electrode-by-electrode basis, we used the raw rather than *z*-scored PC values.

2.9 | Identifying significantly modulated brain regions

A "counts *t*-test" (Ramayya et al., 2015) evaluated the null hypothesis that the proportion of significantly modulated electrodes in a brain region was at chance. We first converted the number of significant electrodes into *z*-scores using a binomial null distribution. The null distribution was based on the total number of electrodes and a false-positive rate = 0.05 (determined from randomization analyses). A one-sample *t*-test evaluated the null hypothesis that the population of positive *z*-scores across subjects was equal to zero. An analogous procedure was conducted for those electrodes with negative *z*-scores.

3 | RESULTS

We recorded ECoG signals from subdural surface and depth electrodes while human subjects listened passively to a sequence of tone bursts. Because the distribution of acoustic frequencies F_1 (1,000 Hz) and F_2 (1,029 Hz) in each sequence was stochastic, the spectral regularity of this auditory stimulus (i.e., the configuration of the F_1 and F_2 tone bursts) changed dynamically. However, because the time between the tone bursts was constant, the sequence's temporal regularity did not change. We analyzed ECoG activity in response to the *last* tone burst of a subsequence (i.e., the test tone burst) as a function of the spectral regularity.

3.1 | Phase consistency—but not power—is modulated by local spectral regularity

In our first analysis, we compared ECoG activity elicited by "regular" subsequences with that elicited by one of two

FIGURE 3 Wide-band frequency relationships between phase consistency (PC) or power and spectral regularity: deviant comparison. The electrocorticographic signal elicited by regular sequences (e.g., F_2—F_2—F_2—F_2) with those that had the same tone-burst frequency except for the last ("deviant") tone burst (e.g., F_1—F_1—F_1—F_2) are compared. Difference in raw PC (a) and log-power (b) values between the regular sequences as a function of subsequence length (SL). In left panels of (a) and (b), black traces and shaded regions depict mean ± *SEM* across subjects, respectively. Horizontal black bars above subplots depict neuronal frequencies for which the difference value is significantly different from zero (signed-rank tests, all $p < 0.05$ with false-detection rate correction). In right panels of (a) and (b), the across-subject mean spectra are plotted together for visual clarity. Panel (c) shows the power (top) and PC (right) spectra for the tone-burst sequences as a function of SL (see legend). The blue data in the left column indicates the power and spectra when the sequences were regular, whereas the grey data in the right column is for the deviant condition. Shading (see legend) indicates SL

different classes of "irregular" subsequences. The regular subsequences were those that contained a single acoustic frequency (e.g., F_2—F_2—F_2—F_2); the bold font indicates the test tone burst in a subsequence. The first class of irregular sequences repeated the same acoustic frequency until the final ("deviant") tone burst (e.g., F_1—F_1—F_1—F_2). The

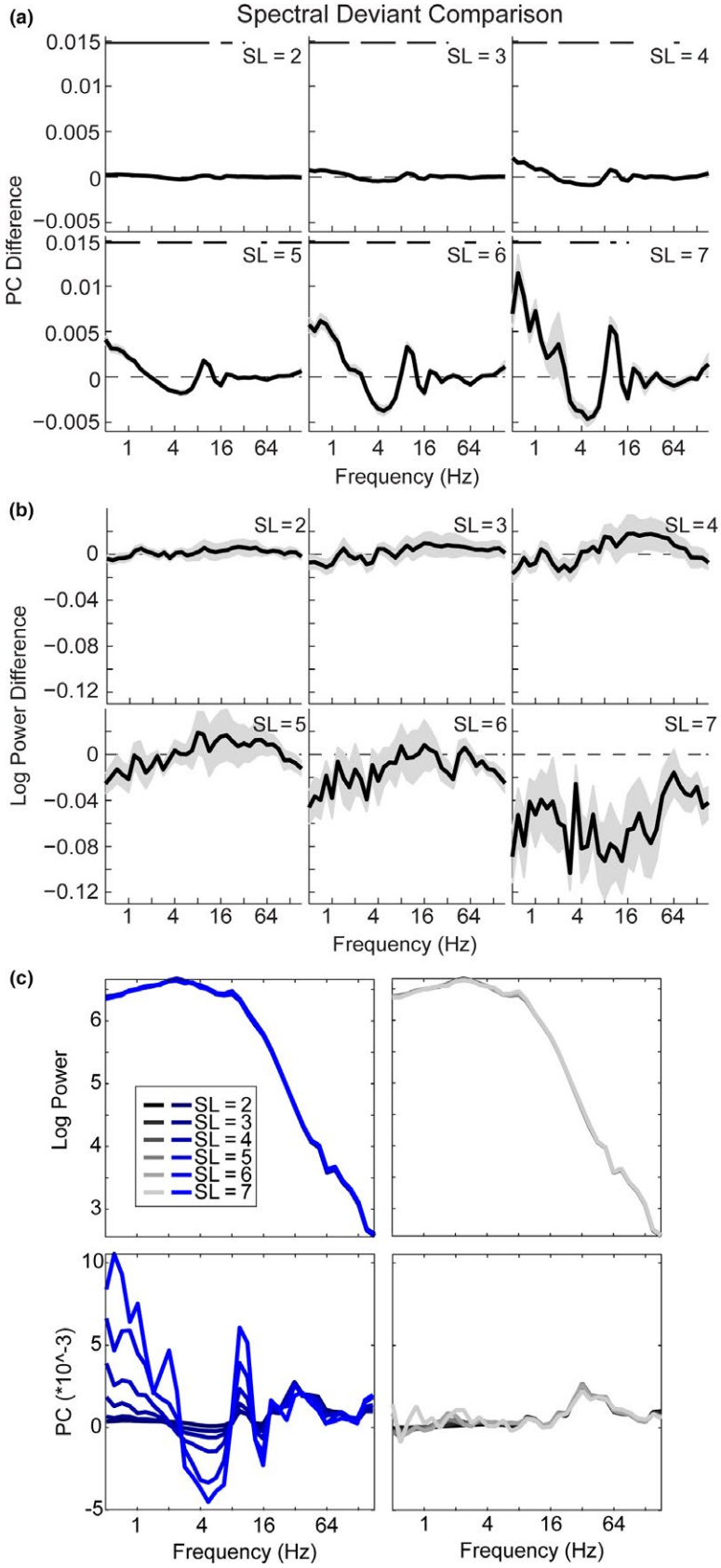

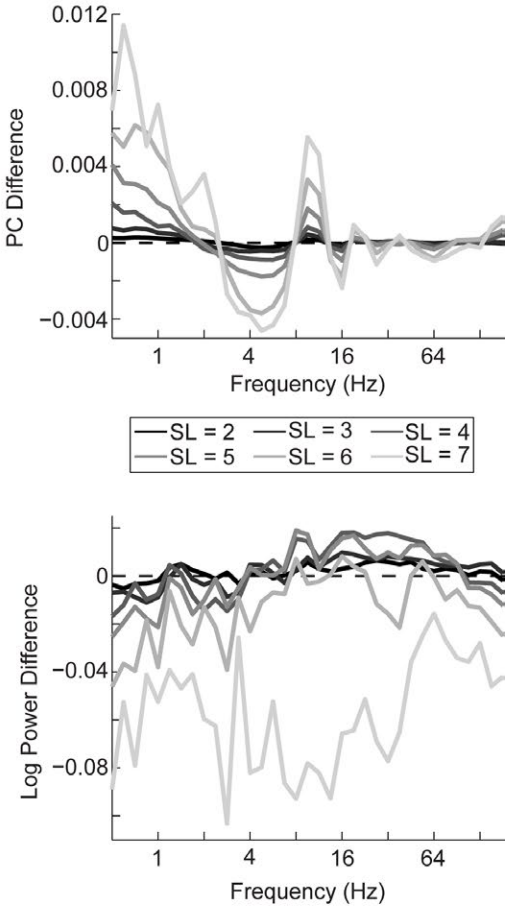

second class of irregular subsequences alternated the acoustic frequency of the tone bursts (e.g., F_1—F_2—F_1—$\mathbf{F_2}$).

The results from this comparison are shown in Figures 3 and 4. In Figures 3a and 4a, we plot a summary of the mean (± *SEM*) within-subject PC differences between the regular subsequences and the two classes of irregular subsequences, respectively, across all electrodes. These differences are plotted as a function of SL (left panels) or combined across SLs (right panels). We note that, in both figures, nearly the entire spectrum was significant for SLs equal to 2 (SL = 2). This occurred because for SL = 2, we have a large number of data points and, hence, substantial statistical power: as a result, small differences can become statistically significant.

We found that, across all tested SLs, spectral regularity consistently modulated PC in distinct neuronal frequency bands (signed-rank tests, df = 11, $N = 12$ subjects, ps < 0.05 for all, FDR corrected across all frequency bands and SLs). In the 10-Hz frequency band (which corresponded to the temporal regularity of the tone-burst sequences), we found larger PC values for the regular subsequences than for the irregular subsequences. We also found similar relative increases in PC in the in the delta-frequency band (<3 Hz) and in the 20-Hz frequency band. On the other hand, in the 5- and 15-Hz bands, we found smaller PC values for the regular subsequences than for the irregular subsequences.

Analogous plots for power differences are shown in Figures 3b and 4b. We could not identify any frequency band in which mean power was modulated by spectral regularity following FDR correction.

3.2 | Phase consistency correlates with the degree of spectral regularity

Because, in the previous sets of analyses, we focused only on a small subset of all possible subsequences, we could not fully assess the extent to which spectral regularity modulated PC and power. To this end, we next quantified the spectral regularity of a subsequence and then tested how well spectral regularity correlated with PC and power.

Our primary metric of regularity was the inverse of Kolmogorov complexity ($1/C_K$; see Section 2). We focused solely on subsequences of tone-burst length = 7 to minimize redundancy in tests across shorter SLs and to maximize the number of unique $1/C_K$ values, which scales linearly with SL. Furthermore, we restricted this analysis to those frequency bands that we previously identified as being modulated by spectral regularity (i.e., delta, 5, 10, 15, and 20 Hz; see Figures 3 and 4).

The results of this analysis are shown in Figures 5 and 6. In Figure 5, we plot (z-scored) PC as a function of $1/C_K$ regularity. Consistent with our previous findings (see Figures 3 and 4), PC was positively correlated with regularity across subjects in the delta, 10-Hz, and 20-Hz frequency bands (Figure 5a; Spearman $\rho = 0.47$, 0.28, and 0.34, respectively; ps = 7.9E–6, 0.0096, and 0.0014 respectively, Holm-Bonferroni corrected; df = 82 for all tests). However, it was negatively correlated with regularity in the 5- and 15-Hz frequency bands (Figure 5b; Spearman $\rho = –0.32$ and –0.52, respectively; ps = 0.0032, and 3.2E–7, respectively, Holm-Bonferroni corrected). We could not identify any differences in the correlation values between the positively correlated or negatively correlated frequency bands (z-tests on Fisher z-transformed correlations: all ps > 0.1; df = 166 for all pairwise tests). The apparent differences in PC values between the subsequences with the largest regularity values (e.g., compare green data points for $1/C_K = 1.662$ in Figure 5) were not reliable across subjects (paired t-tests, ps = 0.57, 0.052, 0.040, 0.017, 0.054, not significant with Holm-Bonferroni correction; df = 11 subjects).

These population trends were also evident at the level of individual subjects (insets in Figure 5a,b). That is, the median individual-subject correlations in the delta and 10-Hz frequency bands were significantly greater than zero (signed-rank tests: ps = 0.033 and 4.9E–4, respectively, Holm-Bonferroni correction; df = 11 subjects). Furthermore, the median correlations in the 5- and 15-Hz frequency bands were significantly <0 (signed-rank tests ps = 0.036 and 9.8E–4, respectively, Holm-Bonferroni corrected).

However, because the largest PC values occurred at the most regular subsequences, significant Spearman-correlation values could have been driven primarily by the responses to these subsequences. To test this idea, we removed the PC values that were generated from the most regular subsequences and reanalyzed the relationship between PC value and regularity. Indeed, we found that for frequency bands higher than the delta band, the across-subject correlation values were generally not significant (all ps > 0.2 except for the 15-Hz frequency band; Spearman $\rho = –0.25$, $p = 0.037$; df = 70 for all tests).

In contrast, a more robust pattern emerged for the delta-band data. When we removed the PC values generated from the most regular subsequence, the correlation remained

FIGURE 4 Regular subsequences (e.g., F2—F2—F2—F2) versus irregular subsequences that alternated in frequency (e.g., F1—F2—F1—F2) are compared. Difference in raw PC (a) and log-power (b) values between the regular sequences as a function of subsequence length (SL). In left panels of (a) and (b), black traces and shaded regions depict mean ± *SEM* across subjects, respectively. Horizontal black bars above subplots depict neuronal frequencies for which the difference value is significantly different from zero (signed-rank tests, all $p < 0.05$ with FDR correction). In right panels of (a) and (b), the across-subject mean spectra are plotted together for visual clarity. In panel (c), the blue data in the left column indicates the power and spectra when the sequences were regular, whereas the grey data in the right column is for the alternating condition. Shading (see legend) indicates subsequence length

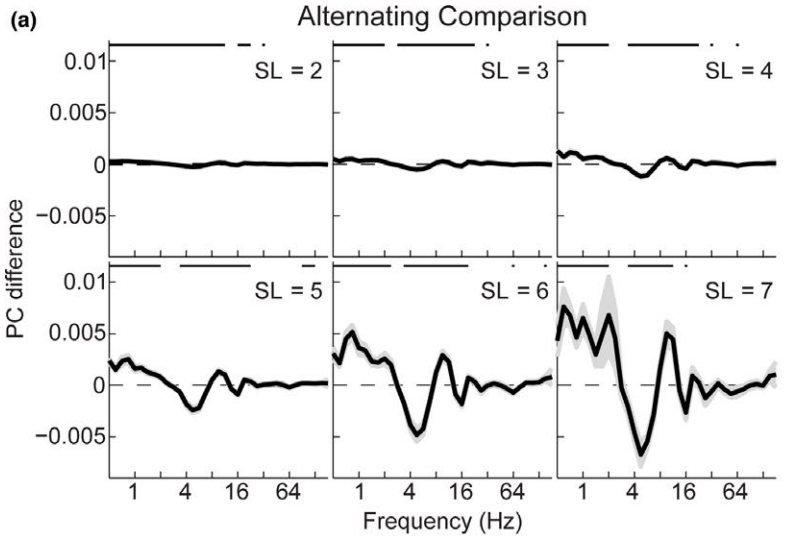
(a)
Alternating Comparison
SL = 2
SL = 3
SL = 4
SL = 5
SL = 6
SL = 7
PC difference
0.01
0.005
0
−0.005
1
4
16
64
Frequency (Hz)

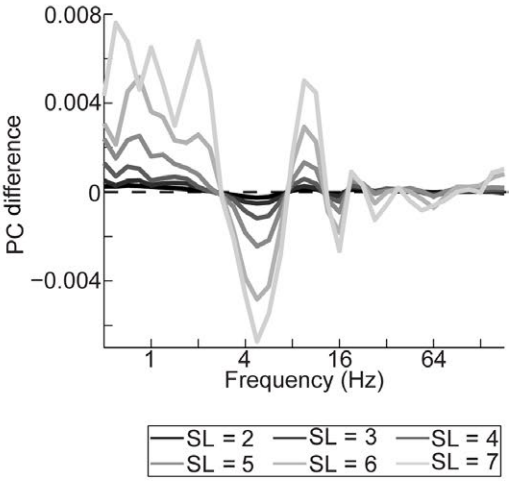
0.008
0.004
0
−0.004
PC difference
1
4
16
64
Frequency (Hz)
SL = 2
SL = 3
SL = 4
SL = 5
SL = 6
SL = 7

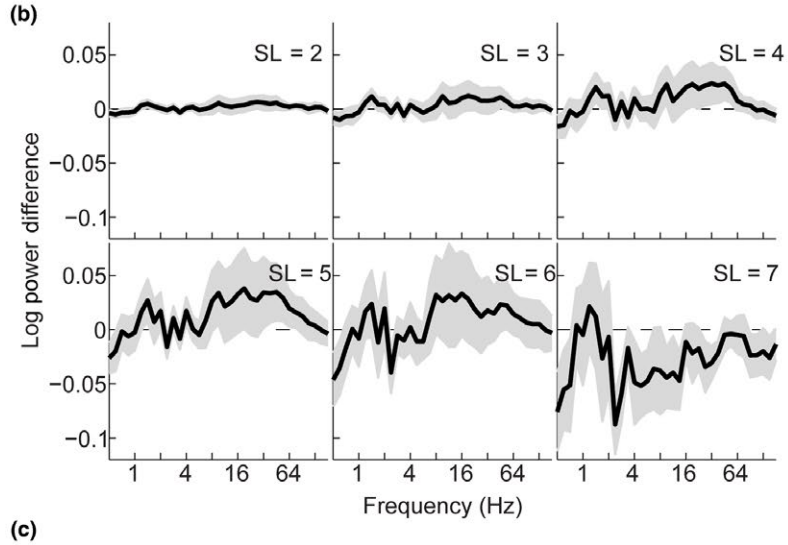
(b)
SL = 2
SL = 3
SL = 4
SL = 5
SL = 6
SL = 7
Log power difference
0.05
0
−0.05
−0.1
1
4
16
64
Frequency (Hz)

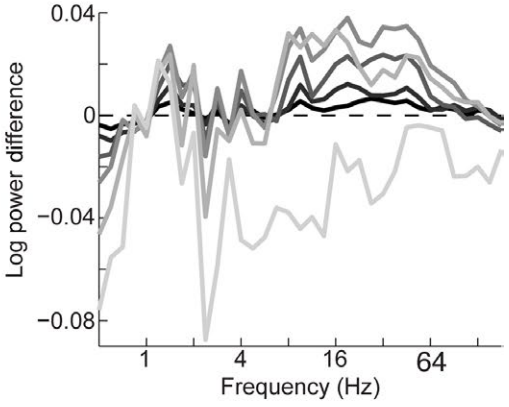
0.04
0
−0.04
−0.08
Log power difference
1
4
16
64
Frequency (Hz)

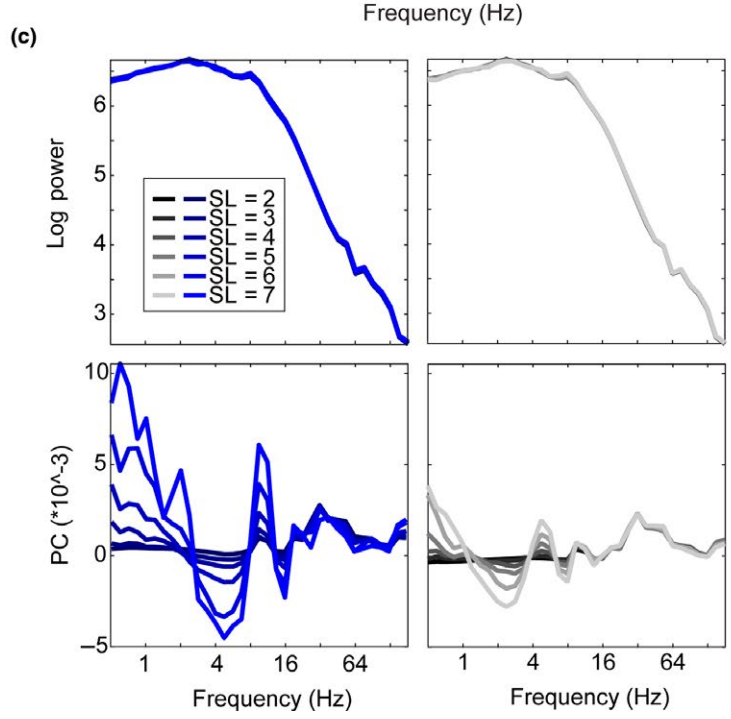
(c)
Log power
SL = 2
SL = 3
SL = 4
SL = 5
SL = 6
SL = 7
PC (*10^-3)
Frequency (Hz)
Frequency (Hz)

significant (Spearman $\rho = 0.37$, $p = 0.0014$). Similarly, this correlation remained significant even when we removed the least regular subsequences from the analysis (Spearman $\rho = 0.53$, $p = 1.7\text{E}{-6}$; df = 70). The correlation in the delta band trended toward significance when we removed the subsequences with the two largest regularity values from the analysis (Spearman $\rho = 0.21$, $p = 0.12$; df = 58). However, when we computed the correlation using the individual subject data, we found that the correlation remained significant even after removing the subsequences with the two largest regularity values (Spearman $\rho = 0.056$, $p = 0.031$; df = 1486). Finally, the correlation remained significant after removing both the most-regular and least-regular subsequences, independent of whether we computed the correlation using PC values from the averaged responses (Spearman $\rho = 0.46$, $p = 2.5\text{E}{-4}$; df = 58) or from the individual subject responses (Spearman $\rho = 0.071$, $p = 0.0067$; df = 1462).

In contrast to these findings for PC, we could not identify any reliable correlations between power and spectral regularity, either in the population trends or at the level of individual subjects (Spearman ps = 0.068, 0.27, 0.75, 0.88, 0.17, 0.92, respectively; df = 82 for all; Figure 6).

Finally, to test the robustness of the correlation between PC in the delta band and $1/C_K$, we reanalyzed the relationship between PC and spectral regularity using three other metrics of regularity (see Analysis of the acoustic-frequency regularity of the tone-burst sequences in Section 2). First, we found that PC values in the delta band were positively correlated with tone-burst proportion (Spearman $\rho = 0.41$, $p = 0.0010$; df = 58). With Shannon entropy (Shannon, 1948; Shannon & Weaver, 1949) as the metric, we found that PC values were negatively correlated with Shannon entropy (Spearman $\rho = -0.53$, $p = 1.2\text{E}{-4}$; df = 46). This finding is consistent with our Kolmogorov complexity metric when we consider that, unlike $1/C_K$, Shannon entropy increases as subsequences become *less* regular. In our final metric, we found, that the delta-band PC values correlated with the number of sub-symmetries (Alexander & Carey, 1968) within each subsequence (Spearman $\rho = 0.40$, $p = 4.8\text{E}{-5}$; df = 94). We could not identify any differences in the magnitudes of the correlation values between these different regularity metrics (pair-wise z-tests on Fisher z-transformed correlations, H_0: correlations are the same, all ps > 0.05). Together, these findings indicate that the correlation between PC alignment was robust to the specific definition of regularity and further strengthened our finding that PC alignment in the delta band correlated with spectral regularity.

3.3 | Phase consistency reflects spectral regularity in multiple brain regions

We found neuronal correlates of spectral regularity in the whole-brain averages of ECoG PC responses. These results could have been due to consistent and widespread activity across the entire brain or the result of strong responses that originated from specific cortical locations (Supporting Information Figures S1 and S2). To differentiate between these two possibilities, we conducted single-electrode analyses to identify regions of cortex that were reliably modulated by spectral regularity. We computed the Spearman correlation

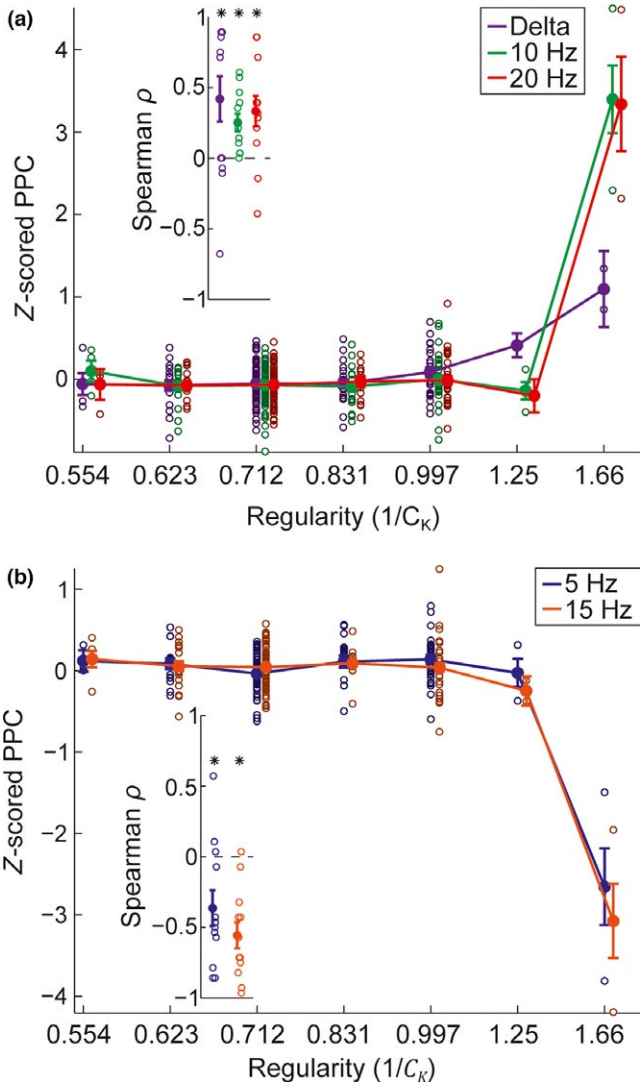

FIGURE 5 Relationship between spectral regularity and phase consistency (PC). *Z*-scored PC as a function of regularity for subsequence length = 7. Panels (a) and (b) depict frequency bands with positive and negative correlations with spectral regularity, respectively. Unfilled data points reflect mean responses to each individual local configuration of F_1 and F_2 across electrodes and subjects. Filled data points with error bars depict across-subject mean and *SEM* responses to all local subsequences with the same spectral-regularity value. Filled data points are connected to highlight trends. Insets depict individual Spearman correlation values for each subject, separately for each frequency band. Asterisks above data points in insets denote frequency bands with significant individual-subject correlations (signed-rank tests: $p < 0.05$ with Holm-Bonferroni correction)

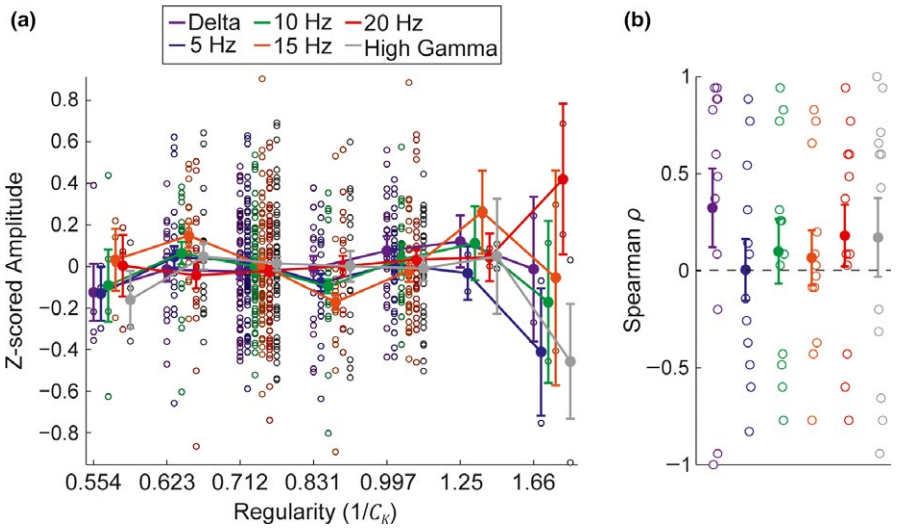

FIGURE 6 Relationship between spectral regularity and amplitude. *Z*-scored log-amplitude as a function of regularity for subsequence length = 7. Data in (a) follow same format as those in the main panels in Fig. 5, with the addition of the high-gamma (HG) responses in gray. Data in (b) follow the same format as those in the insets in Figure 5, with the addition of the HG responses in gray

TABLE 1 Summary correlation statistics for phase consistency (PC) in band-specific analyses

Cortical region by frequency band	Number of electrodes	Number of subjects	Proportion of positively modulated electrodes; counts t-test results	Proportion of negatively modulated electrodes; counts t-test results
Delta				
Frontal cortex	344	11	0.066; $t(10) = 3.5$, $p = 0.0029$*	0.027; $t(10) = 1.1$, $p = 0.15$
Occipital cortex	83	7	0.043; $t(6) = 1.3$, $p = 0.13$	0.043; $t(6) = 1.3$, $p = 0.13$
Parietal cortex	266	12	0.091; $t(11) = 3.0$, $p = 0.0063$*	0.054; $t(11) = 2.6$, $p = 0.012$
Temporal cortex	484	11	0.097; $t(10) = 3.1$, $p = 0.0053$*	0.072; $t(10) = 3.3$, $p = 0.0040$*
5 Hz				
Frontal cortex	344	11	0.024; $t(10) = 1.2$, $p = 0.14$	0.025; $t(10) = 0.73$, $p = 0.24$
Occipital cortex	83	7	0.036; $t(6) = –0.12$, $p = 0.55$	0.091; $t(6) = 1.6$, $p = 0.075$
Parietal cortex	266	12	0.026; $t(11) = 0.71$, $p = 0.25$	0.054; $t(11) = 1.9$, $p = 0.046$
Temporal cortex	484	11	0.049; $t(10) = 1.9$, $p = 0.041$	0.057; $t(10) = 1.8$, $p = 0.047$
10 Hz				
Frontal cortex	344	11	0.029; $t(10) = 0.79$, $p = 0.23$	0.029; $t(10) = 0.51$, $p = 0.31$
Occipital cortex	83	7	0.059; $t(6) = 1.3$, $p = 0.13$	0.038; $t(6) = 0.94$, $p = 0.19$
Parietal cortex	266	12	0.034; $t(11) = 1.3$, $p = 0.12$	0.045; $t(11) = 0.63$, $p = 0.27$
Temporal cortex	484	11	0.093; $t(10) = 4.8$, $p = 0.00038$*	0.030; $t(10) = 0.31$, $p = 0.38$
15 Hz				
Frontal cortex	344	11	0.023; $t(10) = 0.15$, $p = 0.44$	0.048; $t(10) = 2.4$, $p = 0.019$
Occipital cortex	83	7	0; $t(6) = –6.7$, $p = 1.0$	0.11; $t(6) = 2.5$, $p = 0.022$
Parietal cortex	266	12	0.015; $t(11) = –1.1$, $p = 0.85$	0.022; $t(11) = –0.067$, $p = 0.53$
Temporal cortex	484	11	0.030; $t(10) = 0.65$, $p = 0.26$	0.044; $t(10) = 3.1$, $p = 0.0060$
20 Hz				
Frontal cortex	344	11	0.037; $t(10) = 0.92$, $p = 0.19$	0.026; $t(10) = 0.47$, $p = 0.32$
Occipital cortex	83	7	0.031; $t(6) = 0.61$, $p = 0.28$	0.019; $t(6) = –0.21$, $p = 0.58$
Parietal cortex	266	12	0.067; $t(11) = 2.4$, $p = 0.019$	0.065; $t(11) = 1.4$, $p = 0.089$
Temporal cortex	484	11	0.047; $t(10) = 1.9$, $p = 0.046$	0.029; $t(10) = 0.21$, $p = 0.42$

Notes. For each brain region (column 1), we list the number of electrodes (column 2), number of subjects (column 3), proportion of electrodes in which spectral regularity positively (column 4) or negatively (column 5) correlated with PC. Positive t-statistics indicate that the proportion of electrodes with significant correlations was greater than expected, whereas negative t-statistics indicate that the proportion was lower than expected. Asterisks in columns 4 and 5 indicate regions that had a reliable proportion of electrodes (false-detection rate-corrected $p < 0.05$, with Q = 0.05) for which spectral regularity was significantly correlated with PC.

for each electrode, using the raw PC values. With these single-electrode measures, we conducted a counts *t*-test analysis (see Section 2) to localize significant effects across cortex; the results of this analysis are listed in Table 1.

In the delta-frequency band, we found that the frontal, temporal, and parietal cortices had reliable proportions of electrodes that positively tracked spectral regularity (counts *t*-tests; FDR-corrected $p < 0.05$ for all). Additionally, the temporal cortex had a reliable proportion of electrodes that negatively tracked spectral regularity ($p = 0.0040$). In the 10-Hz band and the 15-Hz band, the temporal cortex had a significant proportion of electrodes that both positively ($p = 0.00038$) and negatively ($p = 0.0060$), respectively, correlated with spectral regularity. Thus, although spectral-regularity representation was distributed across the cortex, activity in the temporal cortex appeared to have a more predominate role in tracking spectral regularity.

To better localize these effects, we repeated our counts *t*-test with a finer-grained regional analysis for the subset of frequency bands that were reliably modulated in at least one cortical lobe (Table 2). We found reliable proportions of electrodes that had significant delta-band modulations in the dorsolateral prefrontal cortex, inferior parietal cortex, the banks of the superior temporal sulcus, middle temporal lobe, inferior temporal lobe and the fusiform gyrus (counts *t*-tests, FDR-corrected *p*s < 0.05). In the 10-Hz band, we found that the banks of the superior temporal sulcus, middle temporal lobe, inferior temporal lobe, and fusiform gyrus were also reliably modulated by spectral regularity (counts *t*-tests, FDR-corrected *p*s < 0.05).

A different pattern emerged when we asked whether brain regions contained reliable proportions of electrodes in which power modulations tracked spectral regularity (compare Tables 1 and 3), including brain regions that were modulated by high gamma which we did not see in the whole-brain averages. Unlike the phase relationships, these brain regions contained reliable populations of electrodes that both positively and negatively tracked the relationship between power and regularity. In other words, for the phase modulations, brain regions contained electrodes that consistently (either positively or negatively)

TABLE 2 Fine-grained regional analysis for phase consistency (PC) in band-specific analyses

Region of interest by frequency band	Number of electrodes	Number of subjects	Proportion of positively modulated electrodes; counts t-test results	Proportion of negatively modulated electrodes; counts t-test results
Delta				
Anterior medial frontal	73	6	0.024; $t(5) = -0.22$, $p = 0.60$	0.066; $t(5) = 1.4$, $p = 0.11$
Dorsolateral prefrontal	133	9	0.15; $t(8) = 3.9$, $p = 0.0024$[a]	0.027; $t(8) = 0.83$, $p = 0.22$
Orbitofrontal	25	6	0.074; $t(5) = 1.1$, $p = 0.17$	0.019; $t(5) = 0.15$, $p = 0.44$
Ventrolateral prefrontal	44	8	0.042; $t(7) = 0.22$, $p = 0.42$	0.039; $t(7) = 0.67$, $p = 0.26$
Sensorimotor	49	9	0.055; $t(8) = 1.4$, $p = 0.094$	0.059; $t(8) = 0.67$, $p = 0.26$
Inferior parietal	153	10	0.13; $t(9) = 3.2$, $p = 0.0057$[a]	0.065; $t(9) = 2.1$, $p = 0.032$
Superior parietal	121	11	0.17; $t(10) = 2.5$, $p = 0.018$[b]	0.053; $t(10) = 0.86$, $p = 0.21$
Supramarginal	266	11	0.028; $t(10) = 0.68$, $p = 0.26$	0.087; $t(10) = 1.7$, $p = 0.064$
Medial temporal lobe	36	6	0.055; $t(5) = 0.85$, $p = 0.22$	0.042; $t(5) = 0.86$, $p = 0.22$
Other temporal	136	11	0.097; $t(10) = 3.0$, $p = 0.0063$[a]	0.060; $t(10) = 1.8$, $p = 0.052$
Superior temporal	82	11	0.14; $t(10) = 2.1$, $p = 0.034$	0.063; $t(10) = 2.5$, $p = 0.015$[b]
10 Hz				
Medial temporal lobe	36	6	0.13; $t(5) = 1.5$, $p = 0.10$	0.034; $t(5) = 0.79$, $p = 0.23$
Other temporal	136	11	0.092; $t(10) = 4.3$, $p = 7.3 \times 10^{-4}$[a]	0.034; $t(10) = 0.15$, $p = 0.44$
Superior temporal	82	11	0.11; $t(10) = 2.8$, $p = 0.010$[b]	0.062; $t(10) = 1.0$, $p = 0.16$
15 Hz				
Medial temporal lobe	36	6	0; $t(5) = -5.7$, $p = 1.0$	0.034; $t(5) = 0.79$, $p = 0.23$
Other temporal	136	11	0.029; $t(10) = 0.39$, $p = 0.35$	0.036; $t(10) = 1.5$, $p = 0.088$
Superior temporal	82	11	0.25; $t(10) = 1.1$, $p = 0.15$	0.10; $t(10) = 1.6$, $p = 0.070$

Notes. For each brain region (column 1), we list the number of electrodes (column 2), number of subjects (column 3), proportion of electrodes in which spectral regularity positively (column 4) or negatively (column 5) correlated with PC. Positive t-statistics indicate that the proportion of electrodes with significant correlations was greater than expected, whereas negative t-statistics indicate that the proportion was lower than expected. Asterisks in columns 4 and 5 indicate regions that had a reliable proportion of electrodes (a: false-detection rate [FDR]- corrected $p < 0.05$, with Q = 0.06; b: FDR-corrected $p < 0.05$, with Q = 0.1) for which spectral regularity was significantly correlated with PC.

tracked regularity. In contrast, for power modulations, there was not a consistent relationship.

4 | DISCUSSION

4.1 | Stimulus regularities elicit widespread brain activation

Our findings that the temporal, frontal, and parietal cortices track the spectral regularity of an acoustic stimulus are consistent with a broad set of literature (Besle et al., 2011; Dimitrijevic et al., 2004; Doeller et al., 2003; Garrido, Sahani, & Dolan, 2013; Hsiao et al., 2009; Lakatos et al., 2005, 2013; Lappe, Steinstrater, & Pantev, 2013; Luo et al., 2006; Patel & Balaban, 2000). For example, damage to the dorsolateral prefrontal and parietal cortices reduces the amplitude of the mismatch negativity, which is an evoked potential that tracks the occurrence of novel stimuli whose novelty may be due to changes in spectral regularity (Alain, Woods, & Knight, 1998; Alho, Woods, Algazi, Knight, & Naatanen, 1994). Furtherore, several studies have identified the contribution of the inferior parietal cortex to auditory

TABLE 3 Summary correlation statistics for amplitude in band-specific analyses

Region of interest by frequency band	Number of electrodes	Number of subjects	Proportion of positively modulated electrodes; counts t-test results	Proportion of negatively modulated electrodes; counts t-test results
Delta				
Frontal cortex	344	11	0.20; $t(10) = 4.5$, $p = 0.00054$*	0.12; $t(10) = 3.5$, $p = 0.0027$*
Occipital cortex	83	7	0.11; $t(6) = 2.3$, $p = 0.030$	0.084; $t(6) = 1.9$, $p = 0.052$
Parietal cortex	266	12	0.15; $t(11) = 3.9$, $p = 0.0012$*	0.089; $t(11) = 3.6$, $p = 0.0022$*
Temporal cortex	484	11	0.12; $t(10) = 5.5$, $p = 0.00012$*	0.10; $t(10) = 4.0$, $p = 0.0012$*
5 Hz				
Frontal cortex	344	11	0.036; $t(10) = 1.5$, $p = 0.088$	0.15; $t(10) = 2.4$, $p = 0.020$
Occipital cortex	83	7	0.14; $t(6) = 1.6$, $p = 0.076$	0.13; $t(6) = 2.0$, $p = 0.046$
Parietal cortex	266	12	0.093; $t(11) = 2.3$, $p = 0.021$	0.088; $t(11) = 2.2$, $p = 0.024$
Temporal cortex	484	11	0.11; $t(10) = 2.4$, $p = 0.019$	0.096; $t(10) = 2.5$, $p = 0.017$
10 Hz				
Frontal cortex	344	11	0.040; $t(10) = 1.8$, $p = 0.053$	0.099; $t(10) = 2.2$, $p = 0.028$
Occipital cortex	83	7	0.076; $t(6) = 1.7$, $p = 0.067$	0.075; $t(6) = 0.79$, $p = 0.23$
Parietal cortex	266	12	0.14; $t(11) = 2.6$, $p = 0.012$*	0.11; $t(11) = 2.1$, $p = 0.031$
Temporal cortex	484	11	0.069; $t(10) = 3.4$, $p = 0.0036$*	0.069; $t(10) = 2.7$, $p = 0.010$*
15 Hz				
Frontal cortex	344	11	0.070; $t(10) = 1.8$, $p = 0.049$	0.16; $t(10) = 3.4$, $p = 0.0034$*
Occipital cortex	83	7	0.059; $t(6) = 2.0$, $p = 0.050$	0.11; $t(6) = 1.5$, $p = 0.095$
Parietal cortex	266	12	0.081; $t(11) = 2.1$, $p = 0.028$	0.16; $t(11) = 2.1$, $p = 0.032$
Temporal cortex	484	11	0.049; $t(10) = 1.8$, $p = 0.048$	0.093; $t(10) = 4.3$, $p = 0.00078$*
20 Hz				
Frontal cortex	344	11	0.070; $t(10) = 2.3$, $p = 0.023$	0.042; $t(10) = 1.5$, $p = 0.081$
Occipital cortex	83	7	0.14; $t(6) = 1.8$, $p = 0.062$	0.043; $t(6) = 0.89$, $p = 0.21$
Parietal cortex	266	12	0.068; $t(11) = 1.8$, $p = 0.048$	0.085; $t(11) = 2.5$, $p = 0.016$*
Temporal cortex	484	11	0.071; $t(10) = 2.7$, $p = 0.011$*	0.052; $t(10) = 2.8$, $p = 0.0093$*
High gamma				
Frontal cortex	344	11	0.051; $t(10) = 1.7$, $p = 0.058$	0.091; $t(10) = 2.1$, $p = 0.029$
Occipital cortex	83	7	0.095; $t(6) = 1.8$, $p = 0.064$	0.11; $t(6) = 1.6$, $p = 0.084$
Parietal cortex	266	12	0.026; $t(11) = 0.65$, $p = 0.27$	0.049; $t(11) = 1.9$, $p = 0.044$
Temporal cortex	484	11	0.058; $t(10) = 2.7$, $p = 0.011$*	0.063; $t(10) = 1.9$, $p = 0.043$

Notes. For each region (column 1), we list the number of electrodes (column 2), number of subjects (column 3), proportion of electrodes in which spectral regularity positively (column 4) or negatively (column 5) correlated with electrocorticographic amplitude. Positive t-statistics indicate that the proportion of electrodes with significant correlations was greater than expected, whereas negative t-statistics indicate that the proportion was lower than expected. Asterisks in columns 4 and 5 indicate regions that had a reliable proportion of electrodes (false-detection rate-corrected $p < 0.05$) for which spectral regularity was significantly correlated with amplitude.

scene analysis (Bornkessel-Schlesewsky, Schlesewsky, Small, & Rauschecker, 2015; Cusack, 2005; Dykstra et al., 2011; Giraud et al., 2000; Obleser, Wise, Dresner, & Scott, 2007; Rauschecker, 2011; Teki, Chait, Kumar, von Kriegstein, & Griffiths, 2011; Teki et al., 2016). These wide-spread cortical responses indicate that our findings of a marker for regularity may be a general hallmark of cortical sensory processing (Barascud et al., 2016; Schapiro, Kustner, & Turk-Browne, 2012; Southwell et al., 2017; Turk-Browne, Scholl, Chun, & Johnson, 2009; Ulanovsky, Las, Farkas, & Nelken, 2004; Winkler et al., 2009).

4.2 | Spectral regularity is represented in phase consistency

Spectral regularity was reflected primarily in the degree of PC of ECoG activity. One interpretation of these findings is that increases in spectral regularity systematically affect the tendency of endogenous cortical oscillations to align with the tone bursts (Klimesch, Sauseng, Hanslmayr, Gruber, & Freunberger, 2007; Lakatos et al., 2013; Schroeder & Lakatos, 2009). Alternatively, our findings might reflect nonoscillatory origins related to stimulus-evoked activity that itself is aligned with the tone bursts (Makinen, Tiitinen, & May, 2005). In favor of the former interpretation, delta-frequency power tended to be negatively modulated by the tone-burst sequences (see Figures 3–4), which would not be expected if the tone-burst sequences caused evoked delta-frequency activity. Moreover, if spectral regularity affected the degree of tone-evoked activity, we would have expected to have identified a systematic relationship between amplitude and spectral regularity. However, we did not identify such a relationship.

Yet, it is still possible that, whereas, on average, our results suggest an oscillatory component, individual electrodes may exhibit spectral-regularity-dependent oscillatory or evoked-type responses. Indeed, we found brain regions that had reliable proportions of electrodes with significant correlations between power and spectral regularity (see Table 3). Thus, it is likely that both evoked and oscillatory activity are required to fully explain the present results (Ding, Simon, Shamma, & David, 2016). Further analyses will be required to fully elucidate the differential contributions of each type of activity to spectral-regularity representation (Truccolo, Ding, Knuth, Nakamura, & Bressler, 2002; Xu et al., 2009).

4.3 | Regularity representations versus neuronal adaptation

We interpret our results as evidence of neuronal representations of spectral regularity. However, an alternative interpretation is that our findings reflect neuronal adaptation on short time scales (Eliades et al., 2014; Fishman et al., 2001, 2004; Micheyl et al., 2005; Ulanovsky et al., 2004). The extent to which common neuronal signatures of regularity, such as mismatch negativity, reflect mechanisms of neuronal adaptation versus true regularity representations is an ongoing scientific debate (Fishman, 2014; Fishman & Steinschneider, 2012). Because neuronal adaptation may be modulated by regularity (Todorovic, van Ede, Maris, & de Lange, 2011), at worst, our results reflect neuronal adaptation. Even if this is the case, our results are still important because it extends our understanding of the nature of neuronal adaptation beyond HG-band activity (Eliades et al., 2014; Fishman & Steinschneider, 2012). Our findings also implicate a broad cortical circuit beyond auditory cortex that mediates these numerous correlates of neuronal adaptation (see Tables 1–3).

Nonetheless, several lines of evidence suggest that our findings do reflect a general regularity representation and not simple neuronal adaptation. First, whereas a primary feature of neuronal adaptation is a systematic reduction in HG-band activity to commonly presented stimuli, we were unable to find a reliable effect in HG-band activity across electrodes. Second, we observed both increases and decreases in PC with respect to the most regular subsequences. Indeed, there is no a priori reason to believe that adaptation would affect PC responses differentially as a function of neuronal frequency band. And finally, our results are consistent with previous work that demonstrated oscillatory-phase progression is dependent on the statistical structure of the auditory stimuli (Patel & Balaban, 2000), which is also likely to be independent of neuronal adaptation.

4.4 | Regularity, predictability, and phase consistency

Auditory perception, like perception in other modalities, can be conceptualized as a "predictive" process in which we compare current incoming sensory information with previously learned models of our environment (Arnal & Giraud, 2012; Friston, 2008; Friston & Kiebel, 2009; Sedley et al., 2016; Wacongne et al., 2011). The spectrotemporal regularities of an auditory stimulus are inherently predictive because they probabilistically define the nature of acoustic information over time. As a consequence, it is critical for the auditory system to develop a process to represent spectrotemporal regularity. Indeed, human listeners are capable of reporting changes in both regularities and perceptual grouping within an ongoing auditory stimulus (Bendixen et al., 2013; Elhilali, Xiang, Shamma, & Simon, 2009; Henry, Herrmann, & Obleser, 2014; Teki et al., 2011) and use these predictions to facilitate performance (Costa-Faidella, Baldeweg, Grimm, & Escera, 2011; Henry & Obleser, 2012; Stefanics et al., 2010). The PC of neuronal oscillations with the *temporal* regularity of an auditory stimulus is thought to mediate this functionality (Arnal & Giraud, 2012; Bendixen, SanMiguel, & Schroger, 2012; Besle et al., 2011; Engel, Fries, & Singer,

2001; Lakatos, Karmos, Mehta, Ulbert, & Schroeder, 2008; Lakatos et al., 2005, 2013; Wacongne et al., 2011). Our finding that PC increases with *spectral* regularity suggests that neuronal PC may also be part of a mechanism that contributes to predictive coding.

4.5 | A complex relationship between neuronal-frequency phase consistency and spectral regularity

Based on previous work (Lakatos et al., 2005, 2013; Patel & Balaban, 2000), we expected to find signatures of spectral regularity in the frequency band corresponding to the repetition rate of the tone-burst sequence (that is, 10 Hz). However, we were surprised to find frequency bands that are not trivially related to the acoustic structure of the tone-burst sequences, such as the delta band (Figures 3–5), were also modulated by spectral regularity. It is possible that these modulations in the delta band reflect the tracking of regularities on longer time scales (e.g., repeats of triplets or quadruplets of tone bursts) than the regularities tracked by the 10-Hz PC. This "multiplexing" of regularity representation may be comparable to that seen in speech processing, in which different regularities of a speech signal (e.g., phonemes, words, etc.) are processed simultaneously in different frequency bands (Giraud & Poeppel, 2012; Kerlin, Shahin, & Miller, 2010; Schroeder, Lakatos, Kajikawa, Partan, & Puce, 2008).

A second, non-exclusive possibility is that these delta-band modulations reflect a contribution to sensory selection. In previous work, it was demonstrated that a stimulus with a repetition rate in the delta-band range induces the phase of the delta-band neuronal signal to align with stimulus onset (Schroeder & Lakatos, 2009). One consequence of this alignment is improved behavioral performance (Henry & Obleser, 2012; Lakatos et al., 2016; Stefanics et al., 2010). Although the repetition rate of our stimulus was outside of the delta band, it may be possible that our delta-band oscillations reflect components of this alignment process. Further work is needed elucidate whether stimuli with different repetition rates cause neuronal-PC in different frequency bands and whether this alignment correlates with performance.

Finally, the finding that other neuronal frequency bands (in addition to the 10-Hz and delta bands) were modulated by spectral regularity points to the complex nature of the stimulus representation in the ECoG signal. The tracking of spectral regularity in the 20-Hz band (i.e., the first harmonic of the 10-Hz onset-to-onset interval of the tone-burst sequences) is consistent with previous findings that a temporally regular sequence of events elicits a frequency-following neuronal response at both fundamental and harmonic frequencies (Gomez-Ramirez et al., 2011; Henry & Obleser, 2012; Henry et al., 2014; Nozaradan, Peretz, & Mouraux, 2012). The activity in these harmonic frequency bands also correlates with previously identified aspects of task performance (Gomez-Ramirez et al., 2011; Henry et al., 2014; Nozaradan et al., 2012), suggesting that the 20-Hz modulation may have functional importance. In contrast, to the best of our knowledge, the decrements in PC with increasing spectral regularity in the 5- and 15-Hz frequency bands have not been found previously and require further examination.

ACKNOWLEDGEMENTS

The authors appreciate the critical feedback of Heather Hersh. The authors would also like to thank Erin Beck, Anastasia Lyalenko, and Deborah Levy for helping with consenting and administering the task. Finally, the authors are indebted to the patients who selflessly volunteered to participate in the study. This research was supported by grants from the NIDCD-NIH (YEC), the Boucai Hearing Restoration Fund (YEC), the NIMH-NIH (MJK), and the DARPA Restoring Active Memory (RAM) program (MJK; Cooperative Agreement N66001-14-2-4032). The views, opinions, and/or findings contained in this material are those of the authors and should not be interpreted as representing the official views or policies of the Department of Defense or the U.S. Government.

CONFLICT OF INTEREST

The authors declare no competing interests.

DATA ACCESSIBILITY

Data are available upon request. Files of these stimuli are available at our laboratory website: http://auditoryresearchlaboratory.weebly.com/downloads.html.

AUTHOR CONTRIBUTIONS

AMG collected designed the experiment, collected data, analyzed data, and wrote the manuscript. MRS, AS, RJG, and RBW. KD collected data and wrote the manuscript. MJK and YEC designed the experiment, analyzed data, and wrote the manuscript.

ORCID

Yale E. Cohen http://orcid.org/0000-0002-0830-5162

REFERENCES

Alain, C., Woods, D. L., & Knight, R. T. (1998). A distributed cortical network for auditory sensory memory in humans. *Brain Research*, *812*, 23–37. https://doi.org/10.1016/S0006-8993(98)00851-8

Alexander, C., & Carey, S. (1968). Subsymmetries. *Percept Psychophysics*, *4*, 73–77. https://doi.org/10.3758/BF03209511

Alho, K., Woods, D. L., Algazi, A., Knight, R. T., & Naatanen, R. (1994). Lesions of frontal cortex diminish the auditory mismatch negativity. *Electroencephalography and Clinical Neurophysiology*, *91*, 353–362. https://doi.org/10.1016/0013-4694(94)00173-1

Anderson, K. L., Rajagovindan, R., Ghacibeh, G. A., Meador, K. J., & Ding, M. (2010). Theta oscillations mediate interaction between prefrontal cortex and medial temporal lobe in human memory. *Cerebral Cortex*, *20*, 1604–1612. https://doi.org/10.1093/cercor/bhp223

Arnal, L. H., & Giraud, A. L. (2012). Cortical oscillations and sensory predictions. *Trends Cognitive Science*, *16*, 390–398. https://doi.org/10.1016/j.tics.2012.05.003

Barascud, N., Pearce, M. T., Griffiths, T. D., Friston, K. J., & Chait, M. (2016). Brain responses in humans reveal ideal observer-like sensitivity to complex acoustic patterns. *Proceedings of the National Academy of Sciences of the United States of America*, *113*, E616–E625. https://doi.org/10.1073/pnas.1508523113

Bendixen, A., Bőhm, T. M., Szalárdy, O., Mill, R., Denham, S. L., & Winkler, I. (2013). Different roles of similarity and predictability in auditory stream segregation. *Learning & Perception*, *5*, 37–54. https://doi.org/10.1556/LP.5.2013.Suppl2.4

Bendixen, A., Roeber, U., & Schroger, E. (2007). Regularity extraction and application in dynamic auditory stimulus sequences. *Journal of Cognitive Neuroscience*, *19*, 1664–1677. https://doi.org/10.1162/jocn.2007.19.10.1664

Bendixen, A., SanMiguel, I., & Schroger, E. (2012). Early electrophysiological indicators for predictive processing in audition: A review. *International Journal of Psychophysiology*, *83*, 120–131. https://doi.org/10.1016/j.ijpsycho.2011.08.003

Benjamini, Y., & Hochberg, Y. (1995). Controlling the false discovery rate: A practical and powerful approach to multiple testing. *Journal of the Royal Statistical Society Series B*, *57*, 289–300.

Besle, J., Schevon, C. A., Mehta, A. D., Lakatos, P., Goodman, R. R., McKhann, G. M., … Schroeder, C. E. (2011). Tuning of the human neocortex to the temporal dynamics of attended events. *Journal of Neuroscience*, *31*, 3176–3185. https://doi.org/10.1523/JNEUROSCI.4518-10.2011

Bizley, J. K., & Cohen, Y. E. (2013). The what, where, and how of auditory-object perception. *Nature Reviews Neuroscience*, *14*, 693–707. https://doi.org/10.1038/nrn3565

Bornkessel-Schlesewsky, I., Schlesewsky, M., Small, S. L., & Rauschecker, J. P. (2015). Neurobiological roots of language in primate audition: Common computational properties. *Trends Cognitive Science*, *19*, 142–150. https://doi.org/10.1016/j.tics.2014.12.008

Bregman, A. S. (1990). *Auditory scene analysis*. Boston, MA, USA: MIT Press.

Buracas, G. T., & Boynton, G. M. (2002). Efficient design of event-related fMRI experiments using M-sequences. *NeuroImage*, *16*, 801–813. https://doi.org/10.1006/nimg.2002.1116

Burke, J. F., Zaghloul, K. A., Jacobs, J., Williams, R. B., Sperling, M. R., Sharan, A. D., & Kahana, M. J. (2013). Synchronous and asynchronous theta and gamma activity during episodic memory formation. *Journal of Neuroscience*, *33*, 292–304. https://doi.org/10.1523/JNEUROSCI.2057-12.2013

Costa-Faidella, J., Baldeweg, T., Grimm, S., & Escera, C. (2011). Interactions between "what" and "when" in the auditory system: Temporal predictability enhances repetition suppression. *Journal of Neuroscience*, *31*, 18590–18597. https://doi.org/10.1523/JNEUROSCI.2599-11.2011

Cusack, R. (2005). The intraparietal sulcus and perceptual organization. *Journal of Cognitive Neuroscience*, *17*, 641–651. https://doi.org/10.1162/0898929053467541

Denham, S. L., & Winkler, I. (2006). The role of predictive models in the formation of auditory streams. *Journal of Physiology, Paris*, *100*, 154–170.

Desikan, R. S., Segonne, F., Fischl, B., Quinn, B. T., Dickerson, B. C., Blacker, D., … Killiany, R. J. (2006). An automated labeling system for subdividing the human cerebral cortex on MRI scans into gyral based regions of interest. *NeuroImage*, *31*, 968–980. https://doi.org/10.1016/j.neuroimage.2006.01.021

Dimitrijevic, A., John, M. S., & Picton, T. W. (2004). Auditory steady-state responses and word recognition scores in normal-hearing and hearing-impaired adults. *Ear and Hearing*, *25*, 68–84. https://doi.org/10.1097/01.AUD.0000111545.71693.48

Ding, N., Simon, J. Z., Shamma, S. A., & David, S. V. (2016). Encoding of natural sounds by variance of the cortical local field potential. *Journal of Neurophysiology*, *115*, 2389–2398. https://doi.org/10.1152/jn.00652.2015

Doeller, C. F., Opitz, B., Mecklinger, A., Krick, C., Reith, W., & Schroger, E. (2003). Prefrontal cortex involvement in preattentive auditory deviance detection: Neuroimaging and electrophysiological evidence. *NeuroImage*, *20*, 1270–1282. https://doi.org/10.1016/S1053-8119(03)00389-6

Doelling, K. B., Arnal, L. H., Ghitza, O., & Poeppel, D. (2014). Acoustic landmarks drive delta-theta oscillations to enable speech comprehension by facilitating perceptual parsing. *NeuroImage*, *85*(Pt 2), 761–768. https://doi.org/10.1016/j.neuroimage.2013.06.035

Dykstra, A. R., Halgren, E., Thesen, T., Carlson, C. E., Doyle, W., Madsen, J. R., … Cash, S. S. (2011). Widespread brain areas engaged during a classical auditory streaming task revealed by intracranial EEG. *Frontiers in Human Neuroscience*, *5*, 74.

Elhilali, M., Xiang, J., Shamma, S. A., & Simon, J. Z. (2009). Interaction between attention and bottom-up saliency mediates the representation of foreground and background in an auditory scene. *PLoS Biology*, *7*, e1000129.

Eliades, S. J., Crone, N. E., Anderson, W. S., Ramadoss, D., Lenz, F. A., & Boatman-Reich, D. (2014). Adaptation of high-gamma responses in human auditory association cortex. *Journal of Neurophysiology*, *112*, 2147–2163. https://doi.org/10.1152/jn.00207.2014

Engel, A. K., Fries, P., & Singer, W. (2001). Dynamic predictions: Oscillations and synchrony in top-down processing. *Nature Reviews Neuroscience*, *2*, 704–716. https://doi.org/10.1038/35094565

Fishman, Y. I. (2014). The mechanisms and meaning of the mismatch negativity. *Brain Topography*, *27*, 500–526. https://doi.org/10.1007/s10548-013-0337-3

Fishman, Y. I., Arezzo, J. C., & Steinschneider, M. (2004). Auditory stream segregation in monkey auditory cortex: Effects of frequency separation, presentation rate, and tone duration. *Journal of the Acoustical Society of America*, *116*, 1656–1670. https://doi.org/10.1121/1.1778903

Fishman, Y. I., & Steinschneider, M. (2012). Searching for the mismatch negativity in primary auditory cortex of the awake monkey: Deviance detection or stimulus specific adaptation? *Journal of Neuroscience*, *32*, 15747–15758. https://doi.org/10.1523/JNEUROSCI.2835-12.2012

Fishman, Y. I., Volkov, I. O., Noh, M. D., Garell, P. C., Bakken, H., Arezzo, J. C., … Steinschneider, M. (2001). Consonance and dissonance of musical chords: Neural correlates in auditory cortex of monkeys and humans. *Journal of Neurophysiology*, *86*, 2761–2788. https://doi.org/10.1152/jn.2001.86.6.2761

Friston, K. (2008). Hierarchical models in the brain. *PLoS Computational Biology*, *4*, e1000211.

Friston, K., & Kiebel, S. (2009). Predictive coding under the free-energy principle. *Philosophical Transactions of the Royal Society of London. Series B, Biological Sciences*, *364*, 1211–1221. https://doi.org/10.1098/rstb.2008.0300

Fuentemilla, L., Marco-Pallarés, J., & Grau, C. (2006). Modulation of spectral power and of phase resetting of EEG contributes differentially to the generation of auditory event-related potentials. *Neuroimage*, *30*, 909–916.

Fuentemilla, L., Marco-Pallares, J., Munte, T. F., & Grau, C. (2008). Theta EEG oscillatory activity and auditory change detection. *Brain Research*, *1220*, 93–101. https://doi.org/10.1016/j.brainres.2007.07.079

Garrido, M. I., Sahani, M., & Dolan, R. J. (2013). Outlier responses reflect sensitivity to statistical structure in the human brain. *PLoS Computational Biology*, *9*, e1002999. https://doi.org/10.1371/journal.pcbi.1002999

Giraud, A. L., Lorenzi, C., Ashburner, J., Wable, J., Johnsrude, I., Frackowiak, R., & Kleinschmidt, A. (2000). Representation of the temporal envelope of sounds in the human brain. *Journal of Neurophysiology*, *84*, 1588–1598. https://doi.org/10.1152/jn.2000.84.3.1588

Giraud, A. L., & Poeppel, D. (2012). Cortical oscillations and speech processing: Emerging computational principles and operations. *Nature Neuroscience*, *15*, 511–517. https://doi.org/10.1038/nn.3063

Golomb, S. W. (1982). *Shift register sequences*. Laguna Hills, CA, USA: Aegean Park Press.

Gomez-Ramirez, M., Kelly, S. P., Molholm, S., Sehatpour, P., Schwartz, T. H., & Foxe, J. J. (2011). Oscillatory sensory selection mechanisms during intersensory attention to rhythmic auditory and visual inputs: A human electrocorticographic investigation. *Journal of Neuroscience*, *31*, 18556–18567. https://doi.org/10.1523/JNEUROSCI.2164-11.2011

Henry, M. J., Herrmann, B., & Obleser, J. (2014). Entrained neural oscillations in multiple frequency bands comodulate behavior. *Proceedings of the National Academy of Sciences of the United States of America*, *111*, 14935–14940. https://doi.org/10.1073/pnas.1408741111

Henry, M. J., & Obleser, J. (2012). Frequency modulation entrains slow neural oscillations and optimizes human listening behavior. *Proceedings of the National Academy of Sciences of the United States of America*, *109*, 20095–20100. https://doi.org/10.1073/pnas.1213390109

Hsiao, F. J., Wu, Z. A., Ho, L. T., & Lin, Y. Y. (2009). Theta oscillation during auditory change detection: An MEG study. *Biological Psychology*, *81*, 58–66. https://doi.org/10.1016/j.biopsycho.2009.01.007

Kaspar, F., & Schuster, H. G. (1987). Easily calculable measure for the complexity of spatiotemporal patterns. *Physical Review. A, General Physics*, *36*, 842–848. https://doi.org/10.1103/PhysRevA.36.842

Kerlin, J. R., Shahin, A. J., & Miller, L. M. (2010). Attentional gain control of ongoing cortical speech representations in a "cocktail party. *Journal of Neuroscience*, *13*, 620–628. https://doi.org/10.1523/JNEUROSCI.3631-09.2010

Klimesch, W., Sauseng, P., Hanslmayr, S., Gruber, W., & Freunberger, R. (2007). Event-related phase reorganization may explain evoked neural dynamics. *Neuroscience and Biobehavioral Reviews*, *31*, 1003–1016. https://doi.org/10.1016/j.neubiorev.2007.03.005

Kolmogorov, A. N. (1963). On tables of random numbers. *Sankhyā Series A*, *25*, 369–376.

Kvale, M., & Schreiner, C. E. (1995). Perturbative M-sequence for auditory systems identification. *Acta Acustica*, *81*, 1–6.

Lakatos, P., Barczak, A., Neymotin, S. A., McGinnis, T., Ross, D., Javitt, D. C., & O'Connell, M. N. (2016). Global dynamics of selective attention and its lapses in primary auditory cortex. *Nature Neuroscience*, *19*, 1707–1717. https://doi.org/10.1038/nn.4386

Lakatos, P., Karmos, G., Mehta, A. D., Ulbert, I., & Schroeder, C. E. (2008). Entrainment of neuronal oscillations as a mechanism of attentional selection. *Science*, *320*, 110–113. https://doi.org/10.1126/science.1154735

Lakatos, P., Musacchia, G., O'Connel, M. N., Falchier, A. Y., Javitt, D. C., & Schroeder, C. E. (2013). The spectrotemporal filter mechanism of auditory selective attention. *Neuron*, *77*, 750–761. https://doi.org/10.1016/j.neuron.2012.11.034

Lakatos, P., Shah, A. S., Knuth, K. H., Ulbert, I., Karmos, G., & Schroeder, C. E. (2005). An oscillatory hierarchy controlling neuronal excitability and stimulus processing in the auditory cortex. *Journal of Neurophysiology*, *94*, 1904–1911. https://doi.org/10.1152/jn.00263.2005

Lappe, C., Steinstrater, O., & Pantev, C. (2013). A beamformer analysis of MEG data reveals frontal generators of the musically elicited mismatch negativity. *PLoS ONE*, *8*, e61296. https://doi.org/10.1371/journal.pone.0061296

Lempel, A., & Ziv, J. (1976). On the complexity of finite sequences. *IEEE Transactions on Information Theory*, *IT-22*, 75–81. https://doi.org/10.1109/TIT.1976.1055501

Luo, H., Wang, Y., Poeppel, D., & Simon, J. Z. (2006). Concurrent encoding of frequency and amplitude modulation in human auditory cortex: MEG evidence. *Journal of Neurophysiology*, *96*, 2712–2723. https://doi.org/10.1152/jn.01256.2005

Makinen, V., Tiitinen, H., & May, P. (2005). Auditory event-related responses are generated independently of ongoing brain activity. *NeuroImage*, *24*, 961–968. https://doi.org/10.1016/j.neuroimage.2004.10.020

McDermott, J. (2009). The cocktail party problem. *Current Biology*, *19*, R1024–R1027. https://doi.org/10.1016/j.cub.2009.09.005

Micheyl, C., Tian, B., Carlyon, R. P., & Rauschecker, J. P. (2005). Perceptual organization of tone sequences in the auditory cortex of awake macaques. *Neuron*, *48*, 139–148. https://doi.org/10.1016/j.neuron.2005.08.039

Mukamel, R., Gelbard, H., Arieli, A., Hasson, U., Fried, I., & Malach, R. (2005). Coupling between neuronal firing, field potentials, and FMRI in human auditory cortex. *Science*, *309*, 951–954. https://doi.org/10.1126/science.1110913

Nozaradan, S., Peretz, I., & Mouraux, A. (2012). Selective neuronal entrainment to the beat and meter embedded in a musical rhythm. *Journal of Neuroscience*, *32*, 17572–17581. https://doi.org/10.1523/JNEUROSCI.3203-12.2012

Nunez, P. L., & Srinivasan, R. (2006). *Electric fields of the brain: The neurophysics of EEG*, 2nd ed. New York, NY, USA: Oxford University Press. https://doi.org/10.1093/acprof:oso/9780195050387.001.0001

Obleser, J., Wise, R. J., Dresner, M. A., & Scott, S. K. (2007). Functional integration across brain regions improves speech perception under adverse listening conditions. *Journal of Neuroscience*, *27*, 2283–2289. https://doi.org/10.1523/JNEUROSCI.4663-06.2007

Patel, A. D., & Balaban, E. (2000). Temporal patterns of human cortical activity reflect tone sequence structure. *Nature*, *404*, 80–84. https://doi.org/10.1038/35003577

Ramayya, A. G., Pedisich, I., & Kahana, M. J. (2015). Expectation modulates neural representations of valence throughout the human

brain. *NeuroImage*, *115*, 214–223. https://doi.org/10.1016/j.neuroimage.2015.04.037

Rauschecker, J. P. (2011). An expanded role for the dorsal auditory pathway in sensorimotor control and integration. *Hearing Research*, *271*, 16–25. https://doi.org/10.1016/j.heares.2010.09.001

Ray, S., Crone, N. E., Niebur, E., Franaszczuk, P. J., & Hsiao, S. S. (2008). Neural correlates of high-gamma oscillations (60-200 Hz) in macaque local field potentials and their potential implications in electrocorticography. *Journal of Neuroscience*, *28*, 11526–11536. https://doi.org/10.1523/JNEUROSCI.2848-08.2008

Ray, S., & Maunsell, J. H. (2011). Network rhythms influence the relationship between spike-triggered local field potential and functional connectivity. *Journal of Neuroscience*, *31*, 12674–12682. https://doi.org/10.1523/JNEUROSCI.1856-11.2011

Riecke, L., Sack, A. T., & Schroeder, C. E. (2015). Endogenous delta/theta sound-brain phase entrainment accelerates the buildup of auditory streaming. *Current Biology*, *25*, 3196–3201. https://doi.org/10.1016/j.cub.2015.10.045

Schapiro, A. C., Kustner, L. V., & Turk-Browne, N. B. (2012). Shaping of object representations in the human medial temporal lobe based on temporal regularities. *Current Biology*, *22*, 1622–1627. https://doi.org/10.1016/j.cub.2012.06.056

Schroeder, C. E., & Lakatos, P. (2009). Low-frequency neuronal oscillations as instruments of sensory selection. *Trends in Neurosciences*, *32*, 9–18. https://doi.org/10.1016/j.tins.2008.09.012

Schroeder, C. E., Lakatos, P., Kajikawa, Y., Partan, S., & Puce, A. (2008). Neuronal oscillations and visual amplification of speech. *Trends Cognitive Science*, *12*, 106–113. https://doi.org/10.1016/j.tics.2008.01.002

Sedley, W., Gander, P. E., Kumar, S., Kovach, C. K., Oya, H., Kawasaki, H., … Griffiths, T. D. (2016). Neural signatures of perceptual inference. *Elife*, *5*, e11476. https://doi.org/10.7554/eLife.11476

Shannon, C. E. (1948). A mathematical theory of communication. *The Bell System Technical Journal*, *27*, 379–423. https://doi.org/10.1002/j.1538-7305.1948.tb01338.x

Shannon, C. E., & Weaver, W. (1949). *The mathematical theory of communication*. Champaign, IL: University of Illinois Press.

Shinn-Cunningham, B. G. (2008). Object-based auditory and visual attention. *Trends Cognitive Science*, *12*, 182–186. https://doi.org/10.1016/j.tics.2008.02.003

Southwell, R., Baumann, A., Gal, C., Barascud, N., Friston, K., & Chait, M. (2017). Is predictability salient? A study of attentional capture by auditory patterns. *Philosophical Transactions of the Royal Society of London. Series B, Biological Sciences*, *372*, 20160105. https://doi.org/10.1098/rstb.2016.0105

Stefanics, G., Hangya, B., Hernadi, I., Winkler, I., Lakatos, P., & Ulbert, I. (2010). Phase entrainment of human delta oscillations can mediate the effects of expectation on reaction speed. *Journal of Neuroscience*, *30*, 13578–13585. https://doi.org/10.1523/JNEUROSCI.0703-10.2010

Teki, S., Barascud, N., Picard, S., Payne, C., Griffiths, T. D., & Chait, M. (2016). Neural correlates of auditory figure-ground segregation based on temporal coherence. *Cerebral Cortex*, *26*, 3669–3680.

Teki, S., Chait, M., Kumar, S., von Kriegstein, K., & Griffiths, T. D. (2011). Brain bases for auditory stimulus-driven figure-ground segregation. *Journal of Neuroscience*, *5*, 164–171. https://doi.org/10.1523/JNEUROSCI.3788-10.2011

Todorovic, A., van Ede, F., Maris, E., & de Lange, F. P. (2011). Prior expectation mediates neural adaptation to repeated sounds in the auditory cortex: An MEG study. *Journal of Neuroscience*, *31*, 9118–9123. https://doi.org/10.1523/JNEUROSCI.1425-11.2011

Truccolo, W. A., Ding, M., Knuth, K. H., Nakamura, R., & Bressler, S. L. (2002). Trial-to-trial variability of cortical evoked responses: Implications for the analysis of functional connectivity. *Clinical Neurophysiology*, *113*, 206–226. https://doi.org/10.1016/S1388-2457(01)00739-8

Turk-Browne, N. B., Scholl, B. J., Chun, M. M., & Johnson, M. K. (2009). Neural evidence of statistical learning: Efficient detection of visual regularities without awareness. *Journal of Cognitive Neuroscience*, *21*, 1934–1945. https://doi.org/10.1162/jocn.2009.21131

Ulanovsky, N., Las, L., Farkas, D., & Nelken, I. (2004). Multiple time scales of adaptation in auditory cortex neurons. *Journal of Neuroscience*, *24*, 10440–10453. https://doi.org/10.1523/JNEUROSCI.1905-04.2004

Ulanovsky, N., Las, L., & Nelken, I. (2003). Processing of low-probability sounds by cortical neurons. *Nature Neuroscience*, *6*, 391–398. https://doi.org/10.1038/nn1032

Vinck, M., van Wingerden, M., Womelsdorf, T., Fries, P., & Pennartz, C. M. (2010). The pairwise phase consistency: A bias-free measure of rhythmic neuronal synchronization. *NeuroImage*, *51*, 112–122. https://doi.org/10.1016/j.neuroimage.2010.01.073

Wacongne, C., Labyt, E., van Wassenhove, V., Bekinschtein, T., Naccache, L., & Dehaene, S. (2011). Evidence for a hierarchy of predictions and prediction errors in human cortex. *Proceedings of the National Academy of Sciences of the United States of America*, *108*, 20754–20759. https://doi.org/10.1073/pnas.1117807108

Widmann, A., Schroger, E., & Maess, B. (2015). Digital filter design for electrophysiological data–a practical approach. *Journal of Neuroscience Methods*, *250*, 34–46. https://doi.org/10.1016/j.jneumeth.2014.08.002

Winkler, I., Denham, S. L., & Nelken, I. (2009). Modeling the auditory scene: Predictive regularity representations and perceptual objects. *Trends Cognitive Science*, *13*, 532–540. https://doi.org/10.1016/j.tics.2009.09.003

Winkler, I., Karmos, G., & Naatanen, R. (1996). Adaptive modeling of the unattended acoustic environment reflected in the mismatch negativity event-related potential. *Brain Research*, *742*, 239–252. https://doi.org/10.1016/S0006-8993(96)01008-6

Xu, L., Stoica, P., Li, J., Bressler, S. L., Shao, X., & Ding, M. (2009). ASEO: A method for the simultaneous estimation of single-trial event-related potentials and ongoing brain activities. *IEEE Transactions on Biomedical Engineering*, *56*, 111–121.

SUPPORTING INFORMATION

Additional supporting information may be found online in the Supporting Information section at the end of the article.

How to cite this article: Gifford AM, Sperling MR, Sharan A, et al. Neuronal phase consistency tracks dynamic changes in acoustic spectral regularity. *Eur J Neurosci*. 2018;00:1–20. https://doi.org/10.1111/ejn.14263